Cannabidiol: in vitro drug metabolism, pharmacodynamics, and PBPK modelling

Nattapon Jaisupa

Unit for Pharmacokinetics and Drug Metabolism

Department of Pharmacology

Institute of Neuroscience and Physiology

Sahlgrenska Academy, University of Gothenburg

UNIVERSITY OF GOTHENBURG

Gothenburg 2026

Cover illustration: Optimal cannabidiol exposure is required for controlling neuronal hyperexcitability in epilepsy. Figure created by Nattapon Jaisupa

nattapon.jaispa@gu.se

ISBN 978-91-8069-8115-641-6 (PRINT)
ISBN 978-91-8069-8115-642-3 (PDF)

Printed in Borås, Sweden 2026
Printed by Stema Specialtryck AB

To my family and myself

Cannabidiol: in vitro drug metabolism, pharmacodynamics, and PBPK modelling

Nattapon Jaisupa

Unit for Pharmacokinetic and Drug Metabolism, Department of Pharmacology,
Institute of Neuroscience and Physiology, Sahlgrenska Academy,
University of Gothenburg, Gothenburg, Sweden

ABSTRACT

Cannabidiol (CBD) oral oil solution is approved as add-on treatment for the management of severe childhood epileptic syndromes. Clinical pharmacokinetic studies are few and especially so in the pediatric population. CBD exhibits dose-dependent oral absorption and high pharmacokinetic variability. Therapeutic concentrations are not well established. Potential drug-drug interactions between CBD and antiseizure medications (ASMs) require further study. Any pharmacokinetic algorithm which could predict CBD exposure after varying dosage regimens could be helpful for their optimization, especially in children. A HPLC-MS/MS assay for quantifying CBD, 7-OH-CBD and 7-COOH-CBD was developed and validated. The impact of concomitant ASMs on CBD intrinsic clearance was studied *in vitro* in pooled human liver microsomes (HLMs). Effective and neurotoxic CBD concentrations were examined in human iPSC-derived neuronal culture models by microelectrode array techniques. Finally, a physiologically-based pharmacokinetic (PBPK) model for exposure prediction was developed bottom-up for CBD and its active metabolite 7-OH-CBD and validated based on its predictive performance against available clinical literature data. The bioanalytical assay was shown to be both rapid and sensitive. In HLM incubations, most tested ASM combinations had marginal to moderate effects on CBD hepatic intrinsic clearance with the exception of stiripentol which caused a marked reduction. CYP3A4 substrates reduced the metabolism of 7-OH-CBD. Results in human neuronal *in vitro* cultures indicated preliminary values for effective antiseizure and neurotoxic CBD concentrations. The PBPK model showed good predictive performance in adults and also fair prediction in children and was used for simulation of exposure in children of varying ages as well as effects of combination regimens.

Keywords: cannabidiol, metabolism, pharmacokinetics, pharmacodynamics, physiologically-based pharmacokinetic model

ISBN 978-91-8115-641-6 (PRINT)
ISBN 978-91-8115-642-3 (PDF)

SAMMANFATTNING PÅ SVENSKA

Cannabidiol (CBD) är ett läkemedel som utvinns ur cannabisplantan. Det visar god effekt att förhindra epileptiska anfall. CBD är sedan 2018 godkänt som tilläggsmedicinering vid förebyggande behandling av svår epilepsi hos barn. Även om substansen används kliniskt saknas fortfarande kunskap om dess omhändertagande och omsättning i olika patientgrupper, särskild barn. Ytterligare information om dess kroppsomsättning - så kallat farmakokinetik - är till hjälp vid en mer individanpassad dosering. Inom avhandlingen har därför studerats hur snabbt CBD och dess nedbrytningsprodukt 7-OH-CBD bryts ner av leverenzym. Särskilt studerades i provrör om andra mediciner mot epilepsi kan påverka nedbrytningen av CBD eller dess aktiva produkt 7-OH-CBD. En känslig, selektiv och snabb analysmetod för haltbestämning av CBD och dess två huvudmetaboliter 7-OH-CBD samt 7-COOH-CBD med hjälp av vätskekromatografi kombinerat med masspektrometri utvecklades och kvalitetssäkrades, vilken användes vid dessa försök. Erhållna provrörsresultat extrapolerades till människans förmåga att eliminera dessa substanser.

Vidare undersöktes CBDs effekter i odlade mänskliga nervceller vilka på kemisk väg förmåtts utveckla epilepsiliknande episoder. Genom att registrera nervcellernas elektriska signaler kunde CBDs effekter mätas.

En fysiologiskt baserad matematiskt modell för CBDs omsättning i kroppen utvecklades i syfte att simulera dess blod- och vävnadskoncentrationer. Modellen byggdes baserat på resultat erhållna från tidigare publicerade studier samt egna resultat.

Andra antiepileptiska läkemedel tänkbara vid kombinationsbehandling visade sig ha olika effekter på CBDs nedbrytning. Enstaka läkemedel sänkte eliminationsförmågan, medan andra inte visade större påverkan. Dessa resultat är viktiga för att förskrivare ska kunna välja vilka kombinationer som ger störst nytta med minst biverkningar. Studien på odlade nervceller gav en preliminär indikation vilka koncentrationer som skulle kunna dämpa nervcellers överaktivitet samt den möjligt celltoxiska.

Simulering av den fysiologiskt-baserade matematiska modellen av CBDs omsättning i den mänskliga kroppen var, med hänsyn till hög interindividuell farmakokinetisk variabilitet, i god överensstämmelse med rapporterade resultat från kliniska studier. Modellen kan vara användbar för att optimera CBD-behandling, särskilt hos barn på grund av brist på sådan information i denna population. Modellen är skriven för en öppen plattform varför enkelt att utveckla och fortsatt förbättra.

LIST OF PAPERS

This thesis is based on the following studies, referred to in the text by their Roman numerals.

I. **Jaisupa N**, Ashton M, Birgersson S. A simple, sensitive and rapid bioanalytical method for quantifying cannabidiol (CBD), 7-OH-CBD and 7-COOH-CBD in human plasma. *Bioanalysis*, 2025;17(24):1719-1730.

II. **Jaisupa N**, Ashton M, Birgersson S. Cannabidiol metabolism *in vitro*: the role of antiseizure medications and CYP2C19 genotypes. *Xenobiotica*, 2025;55(3):246-255.

III. **Jaisupa N**, Birgersson S, Ashton M. Potential role of CYP3A4 in determining *in vivo* exposure of cannabidiol (CBD) and its active metabolite 7-OH-CBD: evidence from *in vitro* study. *Submitted*.

IV. **Jaisupa N***, Arthursson E*, Illes S. Cannabidiol pharmacodynamics in human 3D iPSC-neuronal seizure model. *In manuscript*.

* Authors contributed equally

V. **Jaisupa N**, Birgersson S, Ashton M. A transparent physiologically-based pharmacokinetic model for prediction of total and unbound cannabidiol concentrations in adults and children. *Submitted*.

CONTENTS

ABBREVIATIONS

ASMs	Antiseizure medications
BP	Blood-to-plasma ratio
CL_{int}	Intrinsic hepatic clearance
C_{ss}	Concentration at steady state
$C_{u,ss}$	Unbound concentration at steady state
CYP450	Cytochrome P450
EC_{50}	Eliciting 50% of maximal effective concentration
F_{abs}	Fraction of oral dose absorbed
$f_{u,b}$	Unbound fraction in blood
$f_{u,p}$	Unbound fraction in plasma
$f_{u,t,i}$	Unbound fraction in tissue “i”
init (subscript)	initial
inc (subscript)	incubation
HPLC	High performance liquid chromatography
HLMs	Human liver microsomes
K_m	Michaelis-Menten constant
$K_{t,p}$	Tissue-to-plasma partition coefficient
k	Depletion/elimination first order rate constant
MEA	Multielectrode array
MPPGL	Milligram microsomal protein per gram liver

MS	Mass spectrometer
PBPK	Physiologically-based pharmacokinetic (model)
Q_H	Hepatic blood flow
V_{max}	Maximum (metabolic) reaction rate

DEFINITIONS IN SHORT

Blood-to-plasma ratio	The comparative concentration of the drug in whole blood to plasma
Fraction absorbed	Fraction of the dose that is absorbed into the enterocytes
Hepatic intrinsic clearance	Ability of liver to metabolize the drug independently on the protein binding and hepatic blood flow
Hepatic clearance	The volume of blood that is cleared of the drug by the liver over a given period of time
Pharmacodynamics	What the drug does to the body
Pharmacokinetics	What the body does to the drug
Steady state	A condition where the variable remains constant over time
Neuronal network burst	A collective pattern where many neurons inside the network fire rapidly and simultaneously
Volume of distribution	The apparent volume that the drug requires to disperse

1 INTRODUCTION

1.1 EPILEPSY

Epilepsy is a long-term neurological disorder that is attributed to recurrent seizures. More than 50 million people at all ages worldwide suffer from epilepsy. Of those people, approximately 11 million are children below 15 years of age (1).

1.1.1 CLASSIFICATION

The International League Against Epilepsy (ILAE) has established a framework to describe three level of epilepsy including seizure types, epilepsy types, and epilepsy syndromes. Seizures are classified into three types based on the location in the brain where the abnormal electrical firing is originated, which include focal onset, generalized onset and unknown onset. Epilepsy is diagnosed when two or more unprovoked seizures have occurred. In other words, epilepsy is a condition characterized by repetitive or recurrence of accidental seizures. Epilepsy is categorized into four types including generalized, focal, generalized and focal, and unknown epilepsies. The epilepsy syndrome is the term describing a group of symptoms that co-occur and have known causes. Epilepsy syndrome is the third level of epilepsy diagnosis after characterization the types of seizure and epilepsy (2-4). Dravet syndrome, Lennox-Gastaut syndrome, childhood absence epilepsy, juvenile myoclonic epilepsy, juvenile absence epilepsy, and West syndrome are examples of epilepsy syndromes (5, 6).

1.1.2 PRINCIPAL PATHOGENESIS AND SYMPTOMS

The term “seizure” refers to the condition in which groups of neurons in the brain exhibit excessive synchronous activity. The actual molecular mechanisms of seizure remain unclear. Theoretically, an imbalance between inhibition and excitation of neuronal activity underlie the seizure etiology. A dysfunction of ion channels, such as increased function of sodium and calcium channels, or loss of function of GABA receptors, is one of the causes of such imbalanced conditions. Other causes include brain diseases, brain injuries, tumors and stroke (7).

Neurons communicate to other groups of neurons or control other organs, the abnormal function of such affected organs, such as involuntary movement and emotional change, can occur simultaneously during a seizure period.

1.2 DRAVET SYNDROME

Dravet syndrome (DS), first described in 1978 by Charlotte Dravet, is a rare but severe childhood-onset epileptic syndrome. It is also called a severe myoclonic of infancy. The symptoms involve developmental processes in children (8). The incidence of this epileptic syndrome is 1:15000 – 1:40000 accounting for 3-7% of infancy epilepsy (9).

1.2.1 CAUSES AND MANIFESTATIONS

One established cause of DS is a mutation of the gene encoding for voltage-gated sodium channels subtype Nav1.1 (*SCN1A*) which are abundantly expressed on GABA inhibitory interneurons (10). The mutation of this gene results in a loss of function of these GABA inhibitory interneurons, thus increasing excitability of the postsynaptic neurons (11).

DS usually occurs within the early months of life (4-12 months) in the form of febrile seizures, while the other types of seizures such as myoclonus and absence seizures are presented later. The dominant symptoms manifesting in DS include tonic-clonic seizure, myoclonic seizure, absence seizure and focal impaired awareness seizure (8). However, generalized tonic-clonic seizure, tonic seizure and atonic seizure, can also be seen in DS. Since several types of seizures are involved in this syndrome, diversity in electroencephalogram (EEG) in the ictal phase is observed, with generalized spike-wave, polyspike-wave, and focal (or multifocal) epileptiform discharges being the hallmarks (8, 12). Approximately 40% of abnormal EEG were observed in patients aged 0-12 months old but increased to 90% when the children got older (13). Seizures tend to prolong and become a status epilepticus particularly in the patients aged above five years old (14).

1.2.2 PHARMACOLOGICAL TREATMENT FOR SEIZURE SUPPESSION

Resistance to antiseizure medications is one characteristic of DS. Rapid and adequate treatment as well as decreasing factor-induced seizures are the main approaches to reduce a risk of progression to status epilepticus. In case of status epilepticus, intravenous benzodiazepine is the preferable approach (15).

Valproic acid is the first-line antiseizure medication for the maintenance treatment if there are no contraindications (14, 16). Clobazam can be used as monotherapy or combined with valproic acid. However, valproic acid or clobazam monotherapies or a combination of valproic acid and clobazam tend to inadequately control seizures (8, 14). Antiseizure medications currently approved as adjunctive medications for the treatment include stiripentol, fenfluramine and cannabidiol (CBD) (14). Some antiseizure medications such as levetiracetam, topiramate, zonisamide and ethosuximide have not been approved for the indication but show clinical benefits (17). However, some have been reported to worsen the symptoms such as carbamazepine, oxcarbazepine, phenytoin, lamotrigine, vigabatrin, rufinamide and phenobarbital (16).

1.3 LENNOX-GASTAUT SYNDROME

Lennox-Gastaut syndrome (LGS) is one of severe epileptic syndromes found in early life accounting for 1-2% of all epileptic patients (18) or 2-5% of all epilepsy in children (19). Although LGS is a rare disease, the symptoms are severe. LGS is also known as electroclinical syndrome. The characteristics of LGS was first introduced by Gastaut and colleagues. Lennox and Davis later described it as epileptic encephalopathy with diffuse slow spike-wave complex and multiple type of seizures occurring during childhood onset. The nomenclature “Lennox-Gastaut syndrome” was later termed. The definition of LGS was proposed to ILAE in 1989 (20).

1.3.1 CAUSES AND MANIFESTATIONS

There are many precipitating factors that cause LGS which can be divided into two categories: identifiable and unknown causes. Unknown causes account for 65-75% of all cases. The identifiable causes involve structural, genetic, and metabolic factors (18). Examples of structural factor are brain injury and brain malformations. Genetic mutations may be considered when there are no obvious causes (18, 21). Genetic mutations of *SCN2A*, *CDKL5*, *DNM1*, *GABRB3* or *STXBP1* possibly associate with LGS (22).

LGS has been defined by a triad of symptoms including cognitive impairment, multiple types of intractable seizures, and typical EEG abnormalities (19). The hallmark EEG characteristics include the slow spike waves (< 3 Hz) in the interictal phase and paroxysmal fast rhythms (10-20 Hz), particularly during the non-REM sleep (17). Seizures usually start before four years of age. Many

types of seizures can be seen in this syndrome and the common ones are tonic, atonic, myoclonic, atypical absence and generalized tonic-clonic seizures. The seizure types vary among individuals (17, 18).

1.3.2 PHARMACOLOGICAL TREATMENT FOR SEIZURE SUPPESSION

LGS is typically resistant to the pharmacotherapy. To be completely seizure free may not be a major goal of the treatment, but instead to improve patients' quality of life, and to optimize seizure control as well as adverse drug reactions.

To date, monotherapy does not show good efficacy for LGS (23). Valproic acid is a drug of choice and is considered as a first-line drug according to the experts' opinions if there are no contraindications, although it is not officially approved for LGS (17, 18). The antiseizure medications approved for LGS include clobazam, felbamate, rufinamide, lamotrigine and CBD. Some antiseizure medications demonstrating clinical benefits but not approved include zonisamide, levetiracetam, perampanel and fenfluramine (17), whereas some such as phenytoin, carbamazepine, oxcarbazepine, gabapentin, pregabalin, vigabatrin, phenobarbital can aggravate the symptoms (24). In contrast, a study by Feucht and Brantner-Inthaler reported vigabatrin to be efficacious (25).

1.4 TUBEROUS SCLEROSIS COMPLEX

Tuberous sclerosis complex (TSC) is a rare life-long genetic disease with the incidence of 1:6000 (26). The disease causes benign tumor growth in many tissues in the body such as lungs, heart, kidneys, skin and brain.

1.4.1 CAUSES AND MANIFESTATIONS

TSC can be caused by either genetic mutations or abnormality during embryonic development. Mutations in either *TSC1* or *TSC2* genes have been reported to associate with pathogenesis. These genes relate to mechanistic Target of Rapamycin (mTOR) that control the cell growth, and their mutation leads to an abnormality in development and cell growth in the body as tumor. However, 15% of patients develop TSC without *TSC* genes mutation (27). The sign of the disease commonly appears within the first year of life. The symptom severity varies among patients. The patients have high life-threatening risk due to the tumors. Most of TSC cases have epilepsy with different types of seizures (26). Diagnosis of TSC is based on clinical manifestations, family history, diagnostic imaging and ultrasound.

1.4.2 PHARMACOLOGICAL TREATMENT FOR SEIZURE SUPPESSION

The disease cannot be cured currently, but some symptoms can be controlled. Vigabatrin has been approved by the U.S. Food and Drug Administration (FDA) to treat infantile spasm in TSC. Purified CBD was later approved by in 2020 for controlling seizure in TSC (only the maintenance dose of 25 mg/kg/day) (26).

1.5 CANNABIDIOL

1.5.1 PHYSICOCHEMICAL PROPERTIES

Cannabidiol (CBD) is a compound belonging to the cannabinoid family found in the plant genus *Cannabis*. CBD was first extracted from cannabis in 1940, and its structure elucidation was published in 1963 (28). CBD has a very similar chemical structure to delta-9-tetrahydrocannabinol (delta9-THC) consisting of three major parts including a core phenolic ring (resorcinol) linked to a cyclohexene derivative (*d*-limonene) with the molecular weight of 314.46. The natural CBD is available only as a *levo*-isomer or (-)-CBD (**Figure 1**) (29). CBD is a very lipophilic compound with a reported octanol-water partition coefficient (log P) value ranging from 5.9 to 8 with a pK_a value ranging 9.3 to 10.6 (29-31). CBD is extremely poorly soluble in water with a solubility in the range of 0.1-12 µg/mL (32, 33). It is classified in the Biopharmaceutics Classification System (BCS) as a BCS II drug due to its low water solubility along with its high permeability (30).

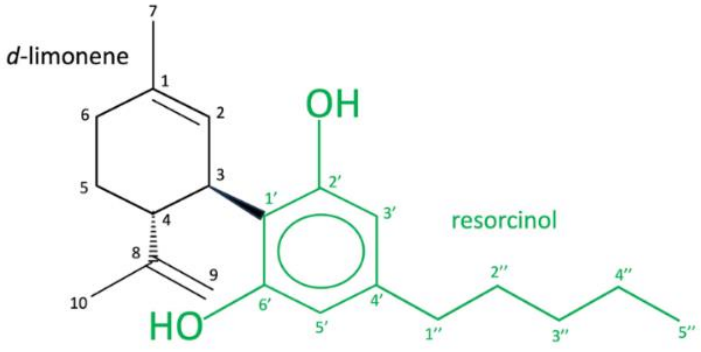

Figure 1. *Chemical structure of levo or (-)-cannabidiol the existing isoform synthesized in cannabis plant.*

1.5.2 BIOACTIVITY OF CBD

Many studies revealed the multiple targets of CBD such as receptors, enzymes and ion channels. CBD acts as negative allosteric modulator on cannabinoid receptor subtype 1 (CB_1) but as a partial agonist or inverse agonist on CB_2 receptor (34). The two hydroxyl groups of CBD can interact with proteins through hydrogen bonds with amino acids such as glutamic acid, glutamine, tyrosine and threonine (35). They are also involved in cytochrome (CYP) 3A inhibition (36).

Unlike THC, CBD binds negligibly to the orthosteric site of both CB_1 and CB_2 receptors, with a very low affinity as indicating by its high value of the inhibition constant (K_i) compared to THC (>4350 nM vs 5-80 nM for CB_1 receptor, and >2400 nM vs 3-75 nM for CB_2 receptor) (37). This could be one reason why CBD does not exert psychoactive effect through the CB_1 receptor. CBD also binds weakly to other receptors, with K_i values higher than 1000 nM, such as serotonin receptor subtypes 1A and 2C ($5\text{-}HT_{1A}$ and $5\text{-}HT_{2C}$), peroxisome proliferator-activated receptor gamma (PPAR-γ), G-protein-coupled receptor 55 (GPR55), μ-opioid receptor (MOR), kappa-opioid receptors (KOR), delta opioid receptor (DOR), dopamine receptor subtype 1 (D_1), histamine receptor subtype 3 (H_3), sigma receptor subtype 2 (σ_2) and alpha receptor subtype 2 (α_2) (29).

CBD is an agonist on the transient receptor potential cation channel subfamily V member 1 (TRPV1), $5\text{-}HT_{1A}$ receptor and PPAR-γ receptor, while acting as an antagonist on GPR55 (34, 38). CBD inhibits fatty acid amide hydrolase (FAAH) which is responsible for anandamide cleavage (39). Due to its multiple targets, CBD has been of interest for study in many indications. CBD has demonstrated anti-inflammatory, anti-nociceptive, neuroprotective, and anxiolytic effects.

1.5.3 CURRENT STATUS OF CBD IN CLINICAL USES

CBD became interesting in the treatment of epilepsy from a case of an American girl, Charlotte, who was diagnosed with DS and suffered from approximately 50 grand mal seizures per day with significant delayed cognition and motor ability. Her seizure frequency was reduced to 2-3 seizure per month after receiving cannabis oil containing a high concentration of CBD in addition to her prescribed antiseizure medications. Her antiseizure medications could later be tapered (40).

Medical CBD, highly purified CBD from hemp, was respectively approved by both FDA and the European Medicines Agency (EMA) in 2018 and 2019 as an adjunctive drug for controlling seizure associated with DS and LGS (41). It was later approved to control seizure associated with TSC (41). CBD is also interesting for the treatment of pharmacoresistant epilepsy (42, 43).

The recommended clinical CBD dose starts from 5 mg/kg/day and is escalated to the maximum maintenance dose of 20 mg/kg/day for DS and LGS. The approved maintenance dose for TSC is 25 mg/kg/day (26). Clinical benefit with good tolerability was also evidenced for high dose of 50 mg/kg/day in some patients (44, 45). Dose escalation is based on clinical responses and adverse drug reactions.

1.5.4 SUGGESTED MECHANISM OF ACTIONS FOR SEIZURE CONTROL AND PHARMACODYNAMICS OF CBD

The actual mechanisms underlying a reduction of neuronal hyperexcitability in seizure are still unclear. The putative mechanisms involve a regulation of neuronal intracellular calcium concentration through the following receptors: antagonism of GPR55, agonism of TRPV1 receptor, and inhibition of equilibrative nucleoside transporter 1 (ENT-1) adenosine reuptake pumps (46, 47). GPR55 couples with the G_q, G_{12} or G_{13} subunits that facilitate an increase in intracellular calcium through inositol triphosphate, RhoA and phospholipase C pathways, respectively. Antagonizing this receptor directly decreases intracellular calcium concentrations. Blockage of ENT-1 adenosine reuptake transporter results in an increase in extracellular adenosine. Adenosine is characterized as an endogenous antiseizure compound in the brain via adenosine receptors A1 and A2. Upon an activation of these two receptor subtypes which are $G_{i/o}$-protein-coupled receptors, calcium influx into presynaptic terminals decreases. Further, activation of A1 and A2 receptors causes postsynaptic hyperpolarization. Activation of the TRPV1 receptor, a ligand-gated cation channel localized in both presynaptic and postsynaptic terminals, promotes the neuronal depolarization, facilitates neurotransmitter release at the presynaptic terminals, and potentiate the firing of postsynaptic neurons (48). However, an *in vitro* study showed that CBD could activate the TRPV1 receptor followed by a rapid desensitization of this receptor (47). Collectively, the inhibition of GPR55 and ENT1 function, or stimulation of TRPV1 receptor could finally lead to a decrease in neuronal excitation.

Furthermore, CBD could block the voltage-dependent calcium and sodium channels, resulting in a reduction of neuronal excitability (49, 50). CBD also modulates GluA1 and GluA2 subunits of glutamate receptor and causes a reduction of neuronal excitability (51). The 3-dimensional structure of CBD and its metabolite 7-COOH-CBD look very similar to phenytoin, a conventional antiseizure medication (52). The structure of 7-COOH-CBD also fits quite well to that of 2E-valproic acid which is an active metabolite of valproic acid (53). This may be another mechanism of CBD to possess antiseizure effect. However, 7-COOH-CBD is reported as an inactive metabolite for antiseizure activity.

The effective antiseizure CBD concentration remains unclear. Results from *in vitro* studies reveal varying effective CBD concentration depending on the target and the used experimental models. In the rat hippocampal slice seizure model induced by 4-aminopyridine (4-AP), CBD reduced the local field potential (LFP) at the concentration of 0.01-100 µM (54). CBD inhibited human voltage-gated sodium channel subtypes Nav1.1-1.7 expressed on HEK-293 cells with the 50% inhibitory concentration (IC_{50}) ranging from 1.9-3.8 µM (55) and; in the same cell type, inhibited human low voltage-activated T-type calcium channels (Cav3) as well as in mouse sensory neurons, in terms of Cav3 currents, with an IC_{50} of approximately 1 µM (56).

In the *in vivo* studies, CBD showed antiseizure activity in many rats or mice seizure models (57). CBD showed a good efficacy to inhibit maximal electroshock and audiogenic seizure in rats with the 50% effective dose (ED_{50}) of 12 and 17 mg/kg, respectively (58). CBD exerted antiseizure activity in 6-Hz model of refractory focal onset and generalized epilepsies in mice with an ED_{50} of 53 mg/kg i.p. (59). CBD could prevent seizure in mice from seizure stimulation using the electroshock seizure model with an EC_{50} in the brain of 7.9 µM, while a 100% effect was observed at the dose 150 mg/kg i.p. corresponding to a brain concentration of 33.7 µM (60).

1.5.5 PHARMACOKINETICS OF CBD

Oral absorption of CBD is limited due to a poor solubility in water (32, 33). An *in vitro* experiment demonstrated a solubility of CBD in artificial intestinal fluid of around 35 to 40 µM (11 to 13 µg/mL) (61). CBD is prone to precipitation in the gastrointestinal tract or may adhere to the enterocyte membranes due to its lipophilicity (62-64). Absorption following an oral administration of CBD oil solution occurs immediate or with a short lag time (65). The first-order absorption rate constant (K_a) has been reported in the

range of 0.005 – 0.0092 min^{-1} (61, 66). Kolli and Hoeng described CBD rate of absorption by a Weilbull function (67). CBD diffuses across the Caco-2 cell monolayer with an apparent permeability (P_{app}) of 5.1 × 10^{-6} cm/s (68), confirming its characterization as a BSC class II drug (67). The fraction absorbed (F_{abs}) tends to decrease at high doses as observed that the area under the concentration-time curve (AUC) was not increasing proportionally to doses (62). Lim *et al*. studied a relationship between CBD dose (750-6000 mg) and bioavailability (F) and created a formula to estimate the bioavailability as: F = 0.065 – 0.048 × ln(Dose in mg/3000) (69). This formula also suggests that the bioavailability is dose-dependent. Administration of CBD with high fat diet caused an increase in AUCs and maximum plasma concentration (C_{max}) (62). The time to maximum concentrations (T_{max}) varied largely among individuals, ranging from 1 to 8 hours (70). CBD plasma C_{max} following an oral ingestion of recommended clinical doses of 5-50 mg/kg/day every 12 hours corresponded to plasma concentration in the range of 7 to 1200 ng/mL (70). Another study reported a mean steady state plasma concentration (random) of approximately 125 ng/mL following the oral administration of medical CBD at the dose 20-25 mg/kg/day (71).

CBD distributes rapidly to organs with high blood supply such as brain, liver, lungs, and heart. It highly accumulates in fatty tissue (72). The mean value of the volume of distribution (V_d) following an intravenous administration of 20 mg deuterated CBD (^{2}H-CBD) in five healthy adults was approximately 32 L/kg (73). CBD plasma concentrations declined multi-exponentially and were best fitted to a three-compartment model (69). A study in postmortem samples revealed the higher CBD concentrations in liver, brain and muscle compared to plasma (74). CBD binds both to plasma protein and erythrocytes, with high binding to albumin >90% (75, 76) and to a less extent (approximately 10%) to erythrocytes. The concentration of CBD measured in plasma was approximately 2-fold higher than that measured in the whole blood (2 ng/mL versus 1.3 ng/mL) suggesting a blood-to-plasma ratio (BP) of approximately 0.65 (77, 78). Unlike THC, CBD does not seem to be a substrate for P-glycoprotein (79).

CBD mainly undergoes phase-I biotransformation in the liver by many CYP450 enzymes, particularly CYP3A4 and CYP2C19. The hydroxylation on the carbon position 7 (methyl group of *d*-limonene moiety) through CYP2C19 pathway yields an active metabolite, 7-OH-CBD (80). It could be implied from an *in vitro* metabolism study using human liver microsomes that approximately 40% of CBD depletion was converted to this active metabolite (80). Phase-II metabolism

subsequently occurs through glucuronidation of the phenolic oxygen as *O*-glucuronide products. CBD proceeds directly to phase-II metabolism to a smaller extent (37). CBD is not a substrate of P-glycoprotein (79).

CBD and its metabolites are excreted from the body mainly through the feces. Around 12% of the parent compound was directly excreted by urine in unchanged form (81). A *O*-glucuronide conjugate product was a major metabolite (13.3%) renally excreted (53).

1.6 PHYSIOLOGICALLY-BASED PHARMACOKINETIC MODELS

Pharmacokinetic modelling has become an important part of drug discovery and development for predicting drug concentrations and pharmacokinetic parameters. Physiologically-based pharmacokinetic (PBPK) models mathematically describe the disposition of a drug in various organs (tissues) in the body and are of interest to predict pharmacokinetic properties of new drugs (82). The model was first proposed in 1937 by Teorell (83). Unlike simple empirical compartment pharmacokinetic models, a PBPK model consists of compartments corresponding to the organs (tissues) in the body linked through the blood circulation system. An advantage of a PBPK model is that anatomical, physiological as well as drug-specific parameters are incorporated. Common tissue compartments included in a PBPK model are brain, heart, kidney, gastrointestinal tract (GUT), liver, lung, muscle, adipose tissue, bone, skin and spleen (84). The rest of the body is represented in a separated compartment in order to obtain mass balance. The additional advantages of PBPK models include an capability to predict outside the studied populations (85) and for personalized medicine (86).

The distribution of a drug in a PBPK model is described by a set of ordinary differential equations (ODE). The rate of drug-tissue distribution can be primarily described by two approaches based on the properties of the drug and the tissue capillaries. The distribution of lipophilic drugs with high permeability can be described by a perfusion-limited approach, whereas permeability-limited kinetics is possibly more appropriate for hydrophilic drugs. The latter is more complicated and needs more specific parameters such as the permeability surface area coefficients, vascular and extravascular volumes to describe tissue distribution.

A PBPK model can be built by three approaches: bottom-up, top-down and middle-out (87). A bottom-up approach, also called *in vitro* - *in vivo* extrapolation, is typically used method (83).

In case of CBD, which is a very lipophilic compound, perfusion-limited distribution was assumed. The change in concentration (C) over time and perfusion-limited disposition are then described by tissue blood flow (Q), tissue volume (V) and the tissue-to-blood partition coefficients ($K_{t,b}$) as shown in the following simplified ODEs:

Non-eliminating tissue;

$$\frac{\mathrm{d}\,C_{tissue}}{\mathrm{dt}} = \frac{\left(Q_{tissue} \times C_{artery} - Q_{tissue} \times \frac{C_{tissue}}{K_{t,b}}\right)}{V_{tissue}}$$

Eliminating tissue (liver);

$$\frac{\mathrm{d}\,C_{liver}}{\mathrm{dt}} = \frac{\left(Q_{liver} \times C_{liver} - Q_{liver} \times \frac{C_{liver}}{K_{t,b\ liver}}\right) - (C_{liver} \times CL_{int} \times f_{u,liver})}{V_{liver}}$$

1.7 SCREENING ANTISEIZURE EFFECT OF COMPOUNDS USING *IN VITRO* MODELS OF SEIZURE-LIKE ACTIVITY

The screening antiseizure efficacy and potency *in vitro* of the candidate compounds is essential before moving to the *in vivo* and clinical studies. The *in vitro* models such as cell cultures, animal brain slice and whole brain preparation (*ex vivo*) are typically used for preclinical investigations (88). However, these *in vitro* models may give rise to questions if they are really reliable in terms of human relevance. In reality, there are no perfect *in vitro* seizure models currently available which 100% relates to seizure occurring in human. However, the existing *in vitro* models can indicate preliminary antiseizure predictive values of the tested compounds.

Since some substantially different intrinsic factors between animal and human such as expression of proteins, receptors, and ion channels, which are the target

of the drugs (89), utilizing cultured human iPSC-derived neurons, one of the most human-related approaches, is of interest. The human cells express the same genotype as observed in the diseases that are advantageous to evaluate the influence of genetics on the drug responses (89). In addition, studies in cultured neurons enables a precise investigation on the cellular mechanisms of pharmacological substances that cannot be performed *in vivo* (90). However, there are some drawbacks of the use of cultured neurons for *in vitro* seizure investigation, for example, the behaviour of electrical activity in ictal and interictal phases between the whole brain and iPSCs are partially different (91). More thorough validations are still required for utilizing iPSCs approach (89).

Establishment of electrophysiological activities relevant to EEG observed in epileptic patients is one important procedure for the investigation. One method to induce seizure-like activity in the brain slice preparations and cultured neurons is to use of epileptogenic substances such as picrotoxin, gabazine, kainic acid, high concentration of potassium, 4-amiopyrine (4AP), and Mg^{2+}-free medium.

Blockage of GABAergic activity by GABA antagonists (gabazine and picrotoxin) or stimulating glutamatergic neuronal transmission (kainic acid) is able to generate high ictal and status epilepticus-like activity (90). Kainic acid induces the seizure activity mimicking the temporal lobe epilepsy (92). High concentration of potassium or potassium channel blockers results in the hyperexcitable state of neurons (93, 94).

Mg^{2+}-free model, the application of medium containing very low Mg^{2+} concentration or concentration of zero, leads to a releasing of Mg^{2+} blocking *N*-methyl-*D*-aspartate (NMDA) receptors and finally triggers massive glutamatergic transmission. Study in hippocampal slice preparation showed that low Mg^{2+} concentration could induce both interictal and ictal-like epileptiform. The early phase of Mg^{2+} deprivation caused population interictal firing, while longer exposure to Mg^{2+} free condition extended a depolarization followed by rhythmic bursting phase. After exposure to Mg^{2+}-free medium for 30-90 minutes, the ictal events were replaced by continuous rhythmic phase. The early ictal event is sometimes sensitive to the treatment, but the rhythmic activity does not adequately respond to standard antiseizure medications (91). In addition, the Mg^{2+}-free seizure model enhances $GABA_A$ receptor internalization and NMDA receptor membrane insertion, which are the features observed in status epilepticus, leading to a designation of the Mg^{2+}-free seizure model as the *in vitro* model for refractory status epilepticus (95).

Further, low Mg^{2+} level *in vivo* has been reported to be clinically relevant by increasing a susceptibility to seizures (96).

In the 4-AP model, 4-AP non-selectively blocks voltage-gated potassium channels (Kv1.1, Kv1.2 and Kv1.3), which play an essential role for repolarization after depolarization leading to an increased intracellular potassium followed by a neuronal depolarization. 4-AP could also induce epileptiform directly by stimulating the excitation of principal neurons, and through the enhancement of glutamate release from presynaptic neurons (97). Seizure-like activity generated by this epileptogenic compound is potent, spontaneous and reproducible. In addition, 4-AP is able to induce epileptiform even in the presence of synaptic inhibition (98). The concentration of 4-AP generally applied for *in vitro* seizure model is 100 μM (99-101). Further, the electrophysiological pattern induced by 4-AP has been reported to be consistent with the electroencephalogram of partial epilepsy or temporal lobe epilepsy (102). A dysfunction of potassium channel has been reported to associate with human epilepsy (103).

1.8 COMBINED ANTISEIZURE EFFECT OF CBD AND ANTISEIZURE MEDICATIONS

Co-medication of CBD with other antiseizure medications may increase the chance of adequate seizure control. The CYP450 inhibiting property of CBD and antiseizure medications may lead to an increase in their exposure. Further, combination of different antiseizure medications with CBD could ideally provide more pronounced antiseizure efficacy due to a variety of mechanisms of action. However, data regarding this aspect is limited.

The study performed by Consroe and Wolkin in rats induced to have seizures by the maximal electroshock and audiogenic approaches showed that the combination of CBD with phenytoin could decrease the phenytoin dose but still obtaining the same magnitude of antiseizure effect (58). In contrast, in the same study, CBD decreased the potency of some antiseizure medications such as clonazepam and ethosuximide.

A study conducted by Golub *et al.* in mice using 6-Hz-induced refractory focal onset generalized seizure model reported that CBD in combination with ganaxolone and midazolam in three different ratios (based on the ED_{50} value) of each drug including 1:1, 1:3 and 3:1 revealed a strong synergistic effect with

a combination index below 0.5. With the combination, the doses of both drugs could be largely reduced compared to the condition when they were applied alone (59).

The study by Rana *et al*. revealed that CBD in combination with clobazam provided a synergistic effect to prevent seizure in mice induced by the maximal electroshock with a combination index less than 1 based on the combination ratios of effective brain concentration of each drug (60).

In a meta-analysis of four randomized controlled trials, it was concluded that clobazam co-medicated with CBD (10 or 20 mg/kg/day) exhibited superior antiseizure efficacy to ~~a~~ co-medication with placebo. However, this study did not evaluate the effective dose ratio of these two medications (104).

2 AIM

The main aim of this thesis was to investigate the metabolism of CBD and its active metabolite 7-OH-CBD with and without the presence of antiseizure medications as well as effective concentrations *in vitro*, and use such information as input in a pharmacokinetic algorithm/model for prediction of CBD exposure *in vivo* with the ultimate aim to optimize pediatric dosing.

The specific aims were:

1. To develop a simple and effective bioanalytical method for rapidly quantifying CBD and two metabolites; 7-OH-CBD and 7-COOH-CBD using high performance liquid chromatography coupled with mass spectrometer **(Paper I)**.
2. To evaluate the impacts of antiseizure medications and moderate-activity genotyped CYP2C19 on *in vitro* CBD metabolism in human liver microsomes **(Paper II)**.
3. To investigate the impact of antiseizure medication CYP3A4 substrates on *in vivo* exposure of CBD and 7-OH-CBD **(Paper III)**.
4. To assess the effective antiseizure and neurotoxic concentrations of CBD in human iPSC-derived 3D neuronal culture **(Paper IV)**.
5. To develop and validate a physiologically-based pharmacokinetic (PBPK) model for CBD and 7-OH-CBD **(Paper V)**.

3 METHODS

3.1 BIOANALYTICAL METHOD DEVELOPMENT (PAPER I)

A simple but sensitive and rapid bioanalytical method for quantifying CBD and its metabolites 7-OH-CBD and 7-COOH-CBD was developed and validated using human plasma as biological matrix.

3.1.1 EVALUATION OF COMPOUND SPECIFIC PARAMETERS FOR MASS SPECTROMETRY

All analytes were first examined for their suitable quantifier transitions under positive or negative ionization modes by a direct infusion of methanolic solution (100 µM) of the analytes. The parameters collision gas (CAD), curtain gas (CUR), ion source gas 1 (GS1) and ion source gas 2 (GS2) were respectively fixed at 9 psi, 50 psi, 40 psi and 70 psi based upon the values reported in the literature, while ramping and optimizing the declustering potential (DP), entrance potential (EP), collision energy (CE), cell exit potential (EXP), ion spray voltage (IS) and temperature.

3.1.2 HIGH-PERFORMANCE LIQUID CHROMATOGRAPHY COUPLED WITH MASS SPECTROMETER

Analysis was performed on a HPLC system consisting of an autosampler (PAL HTC, CTC Analytics AG, Zwingen, Switzerland), two pumps (PE-200 LC, Perkin Elmer, Waltham, MA, USA) connected to an API 4000 triple quadrupole mass spectrometer equipped with electrospray ionization source (AB Sciex, Framingham, MA, USA).

3.1.3 CHROMATOGRAPHIC CONDITIONS

All the analytes were evaluated for their separation in different chromatographic columns including two BDS Hypersil C-18 column, particle size 3 µm, diameter 4.6 mm (50 and 100 mm in length) (Part No 28103-104630, Thermo Scientific), and Ascentis Express C18 column (5 cm × 4.6 mm, 2.7 µm, BL:S13079, Col:USUT00383, Cat#53826-U, SUPELCO). The column temperature was controlled at temperature of 20°C. Various mobile phases were examined for elution including: two aqueous phases (0.1% formic acid in water or ammonium acetate in water), and two solvents as organic phase

(methanol and acetonitrile), mixed at different ratios. The following parameters were examined; isocratic versus gradient elution, flow rates of 0.3 versus 0.4 mL/min, injected volumes of 5 versus 10 µL, and two versus three times of needle washing.

3.1.4 STANDARD PLASMA SAMPLE PREPARATION ANALYTE EXTRACTION

To a volume of 100 µL of blank plasma was added 10 µL of methanolic solution of each analyte, previously prepared at the concentration 10-fold higher than the desired final concentration in plasma. An equal volume of cold acetonitrile containing internal standards (100 nM CBD-D3 for CBD and 7-OH-CBD, or 200 nM 7-COOH-CBD-D3 for 7-COOH-CBD) was added and mixed to precipitate plasma proteins and to extract the analytes. The mixture was centrifuged at 10000*g* for 5 minutes. The supernatant was collected and evaporated under gentle flow air at 35°C. Dried residuals were reconstituted with 50 µL acetonitrile, mixed and centrifuged under the same condition. Approximately 40 µL of supernatants were collected for analysis.

3.1.5 DATA HANDLING AND ANALYSIS

The detector responses as the peak area ratio of the analyte to the internal standard were used for analysis. Data handling was performed in Analyst software version 1.6.3 (AB Sciex, Framingham, MA, USA).

3.1.6 VALIDATION

The method was validated for linearity, sensitivity, accuracy, precision, selectivity, specificity, carryover, dilution integrity, long-term stability, freeze-thaw stability and recovery according to guidance for bioanalytical method validation for industry 2018 issued by FDA (105).

3.2 EVALUATION OF THE IMPACT OF ANTI-SEIZURE MEDICATIONS AND MODERATE-ACTIVITY CYP2C19 GENOTYPES ON CBD METABOLISM (PAPER II)

The metabolic effects of antiseizure medications as well as moderate-activity CYP2C19 genotypes on CBD metabolism was evaluated using pooled human liver microsomes (HLMs). The obtained intrinsic clearances were used to scale and predict changes in the steady-state CBD concentration *in vivo*.

3.2.1 EXPERIMENT DESIGN

Studies on CBD *in vitro* metabolism was performed in HLMs pooled from 200 donors, expected to carry wild-type CYP450 enzymes (Xenotech, Kansas City, KS, USA) containing 0.1 mg/microsomal protein/mL (or 0.377 nmol CYP450/mL). Incubation volume were 1 mL. Various CBD initial concentrations (400-6000 nM) with and without antiseizure medications (valproic acid, clobazam, stiripentol and topiramate) was pre-incubated with HLMs before starting the metabolic reaction. For the moderated-activity genotyped CYP2C19 (**1/*2* or **1/*4*), only CBD without antiseizure medications was examined.

3.2.2 METABOLIC REACTION AND SAMPLING

Procedures followed previous literature with slight modifications (106, 107). Briefly, after 10-min preincubation of CBD with/without antiseizure medications with HLMs at 37ºC in gently agitating water bath, the metabolism was initiated by adding NADPH solution (rapidSTART, Xenotech, Kansas City, KS, USA) to gain the final concentration of 1.2 mM. Aliquots of 100 µL of the incubation mixture were sampled at nine time points: 0 (immediately after initiating the reaction), 2.5, 5, 10, 15, 20, 30, 45 and 60 minutes to determine CBD, 7-OH-CBD and 7-COOH-CBD contents using the previously described bioanalytical method (section 3.1).

3.2.3 CALCULATION OF CBD DEPLETION AND METABOLITE FORMATION

The initial CBD depletion rate constant (k_{init}) at each CBD initial concentration was estimated by fitting a mono-exponential function to the observed response-time data (time 0 to 10-15 minutes) using Microsoft Excel (Solver).

This k_{int} value together with CBD initial concentration (CBD_{init}) and volume of incubation mixture (Vol_{inc}) were further used for calculating initial depletion rate (nmol/min/nmol CYP450) with a correction the amount of CYP450 enzymes in the incubation mixture ($CYP450_{inc}$) as follow:

$$\text{Initial depletion rate } (V_{init}) = \frac{CBD_{init} \times k_{init} \times Vol_{inc}}{CYP450_{inc}}$$

To calculate incubation half-lives, the depletion rate constant (k) was instead estimated from the observed response-time data from 0-30 minutes. The depletion half-life was further calculated as follows:

$$\text{Incubation half} - \text{life (min)} = \frac{\ln 2}{k}$$

The metabolite formation at each CBD initial concentration was estimated using a power function (response = $a \times time^b$) fitted to the observed response from time 0 to 20 minutes (Microsoft Excel, Solver). The initial formation rate (arbitrary unit/min/nmol CYP450) was calculated at 2.5 minutes after initiating the reaction using the differentiated form of the power function as follows:

$$\text{Initial formation rate (at 2.5 min)} = b \times a \times 2.5^{(b-1)}$$

where a and b are constants obtained from the fitting. The resulting value was further corrected by the amount of CYP450 enzymes in the incubation mixture.

3.2.4 ESTIMATION OF INTRINSIC CLEARANCE AND HEPATIC CLEARANCE

The *in vitro* intrinsic clearance was ($CL_{int,vt}$) estimated from the maximum velocity of depletion (V_{max}) and the Michaelis-Menten constant (K_m) as follows (108):

$$CL_{int,vt}(\mu L/min/nmol\ CYP450) = \frac{V_{max}}{K_m}$$

where V_{max} and K_m were derived from the fitting of a simple Michaelis-Menten model using V_{init} and their corresponding concentrations (C) as follows:

$$V_{init}\ (nmol/min/nmol\ CYP450) = \frac{V_{max} \times C}{K_m + C}$$

The *in vivo* intrinsic clearance ($CL_{int,vv}$) was further scaled from the $CL_{int,vt}$ using nmol CYP450 per mg microsomal protein (CYP450), milligram microsomal protein per gram liver (MPPGL), unbound fraction in incubation mixture ($f_{u,inc}$), and liver weight (LW) as follow (with the $f_{u,inc}$ assumed equal to 1):

$$\mathrm{CL_{int,vv}(L/min)} = \frac{\mathrm{CL_{int,vt}\ (L/min/nmol\ CYP450)}}{\mathrm{f_{u,inc}}} \times \mathrm{CYP450} \times \mathrm{MPPGL} \times \mathrm{LW\ (gram)}$$

The hepatic clearance (CL_H) was subsequently estimated, based on the well-stirred model of hepatic extraction (E_H), using $CL_{int,vv}$ together with the hepatic blood flow (Q_H) and blood unbound fraction ($f_{u,b}$) as follows:

$$\mathrm{CL_H = Q_H \times E_H}$$

$$\mathrm{E_H} = \frac{\mathrm{f_{u,b} \times CL_{int,vv}}}{\mathrm{Q_H + (f_{u,b} \times CL_{int,vv})}}$$

3.2.5 PREDICTION OF AVERAGE CBD UNBOUND CONCENTRATION AT STEADY-STATE

The average unbound concentration at the steady state ($C_{u,ss}$) of CBD was calculated using a formula derived based on the well-stirred model of hepatic extraction as follows:

$$\mathrm{C_{u,ss}} = \frac{\mathrm{F_{abs} \times Dose\ rate}}{\mathrm{CL_{int,vv}}}$$

3.3 EVALUATION OF POTENTIAL IMPACT OF ANTISEIZURE MEDICATION CYP3A4 SUBSTRATES ON METABOLISM OF CBD AND 7-OH-CBD (PAPER III)

The influence of CYP3A4-inhibiting antiseizure medications on the metabolism of CBD and 7-OH-CBD was determined *in vitro* using pooled HLMs to predict the exposure *in vivo*.

3.3.1 EXPERIMENT DESIGNS, METABOLIC REACTION AND ANALYSIS

The metabolism of CBD (100 nM) in the presence of six combinations of antiseizure medication was determined in HLMs pooled from 200 donors: CBD alone, CBD + stiripentol, CBD + valproic acid + clobazam + topiramate, CBD + valproic acid + clobazam + topiramate + zonisamide, CBD + valproic acid + clobazam + topiramate + felbamate, and CBD + zonisamide + felbamate + ethosuximide + perampanel. In the last condition, all antiseizure medications are mainly metabolized by CYP3A4. The incubation procedure was as previously described (section 3.2). The incubation mixture was sampled and analyzed at seven time points including 0, 5, 10, 15, 20, 30, 45 and 60 minutes using the method previously described (section 3.1).

3.3.2 DETERMINATION OF INTRINSIC CLEARANCES

The $CL_{int,vt}$ of CBD was calculated using the depletion rate constant (k) obtained from mono-exponential fitting using all the observed response-time points (0-60 minutes), whereas the $CL_{int,vt}$ of 7-OH-CBD was calculated from the k value estimated from data points at elimination phase (time 20-60 minutes). The $CL_{int,vt}$ was calculated using the k value and Vol_{inc} as follows:

$$\mathrm{CL_{int,vt}} = \mathrm{k} \times \mathrm{Vol_{inc}}$$

The initial metabolite formation rates were described by a power function and determined at 5 minutes after initiating the reaction by the differentiated power function as previous mentioned (section 3.2.3)

3.4 PHARMACODYNAMIC EVALUATION OF CBD IN HUMAN IPSC-DERIVED 3D NEURAL MODEL OF ACUTE SEIZURE ACTIVITY (PAPER IV)

In vitro investigations were conducted to determine the effective antiseizure and neurotoxic concentrations of CBD in human iPSC-derived neuronal networks and to characterize its pharmacodynamic profile, including efficacy, potency, time to maximum effect, reversibility, and neurotoxicity.

3.4.1 CULTIVATION OF HUMAN IPSC-DERIVED NEURONS

Human iPSC-neural stem cells were produced from a human iPSC line by the DUAL-SMAD inhibition protocol (109), and stocks of hiPSC-derived neural stem cells were cryopreserved until further use. Stocks of iPSC-neural stem cells were thawed and grown on a Poly-L-Ornithine/Laminin coated 3.5-cm plates and cultured in neural culture media. Within 7 to 10 days human 3D-neural aggregates are formed. Five to 10 neuronal aggregates were transferred to the Poly-L-Ornithine/Laminin-coated 96-well multielectrode array (MEA) plates (Multi Channel Systems MCS GmbH, Reutlingen Germany), followed by neuronal differentiation process in supplemented BrainPhys medium. The medium changes were performed once weekly. The neuronal activity was recorded with microelectrodes and Multiwell-screen software. Spontaneous synchronous neuronal network activity was offline analysed using the Multiwell-Analyzer (Multi Channel Systems MCS GmbH, Reutlingen, Germany). For further details regarding the methodology and procedures see elsewhere (110).

3.4.2 INDUCTION OF SEIZURE-LIKE ACTIVITY

Two acute seizure models; 4-aminopyridine (4-AP) and Mg^{2+}-free medium (artificial cerebrospinal fluid; aCSF) were employed for investigations. In the first model, a 4-AP working solution prepared in sterile distilled water was added to cultures after medium change to yield a final 4-AP concentration of 100 µM. In the Mg^{2+}-free model, the culture medium was removed and replaced directly with Mg^{2+}-free aCSF. The neural cultures were incubated for 45 minutes, and recording the activity as seizure baseline before further investigation.

3.4.3 ASSESSMENT OF CBD EFFICACY AND POTENCY

CBD working solution was added to neural cultures (3.4.2) to obtain the final CBD concentration of 1, 2.5, 5 and 10 µM, with the end concentration of the co-solvent DMSO limited below 0.1%. For the 4-AP model, a 10-minute neuronal activity recording was consecutively measured at four time points; immediately after CBD addition (0) followed by 20, 40, and 60 minutes post CBD incubation. For the Mg^{2+}-free model, the recordings were performed only at baseline and at 60 minutes post CBD incubation. CBD efficacy was evaluated by means of a 50% effective concentration (EC_{50}) using the log-logistic concentration-response model fitted to the concentration-efficacy data (R software).

3.4.4 REVESIBILITY AND NEUROTOXICITY ASSESSMENT OF CBD

Neuronal activity reversibility was examined only in the 4-AP model. After the last recording at 60 minutes, the cultures underwent repeated washing, followed by incubation in fresh culture medium, and activity was measured again 24 hours later. The absence of neuronal activity was interpreted as evidence that CBD has toxic effects on human neuronal functionality.

3.5 DEVELOPMENT OF A PHYSIOLOGICALLY-BASED PHARMACOKINETIC MODEL FOR CANNABIDIOL (PAPER V)

A whole-body physiologically-based pharmacokinetic (PBPK) model of CBD was developed bottom-up to simulate CBD concentration-time profiles following CBD administration.

3.5.1 MODEL STRUCTURE

The model consisted of twelve compartments, including lungs, heart, brain, kidneys, liver, gastrointestinal tract (GUT), spleen, adipose tissues, bone, muscles, skin, and the rest of the body, connected by venous and arterial blood circulation (**Figure 2**). In the model for oral administration, the GUT compartment was subdivided into eight sections including stomach (dose compartment), duodenum, jejunum1, jejunum2, iluem1, ileum2, ileum3 and ascending colon.

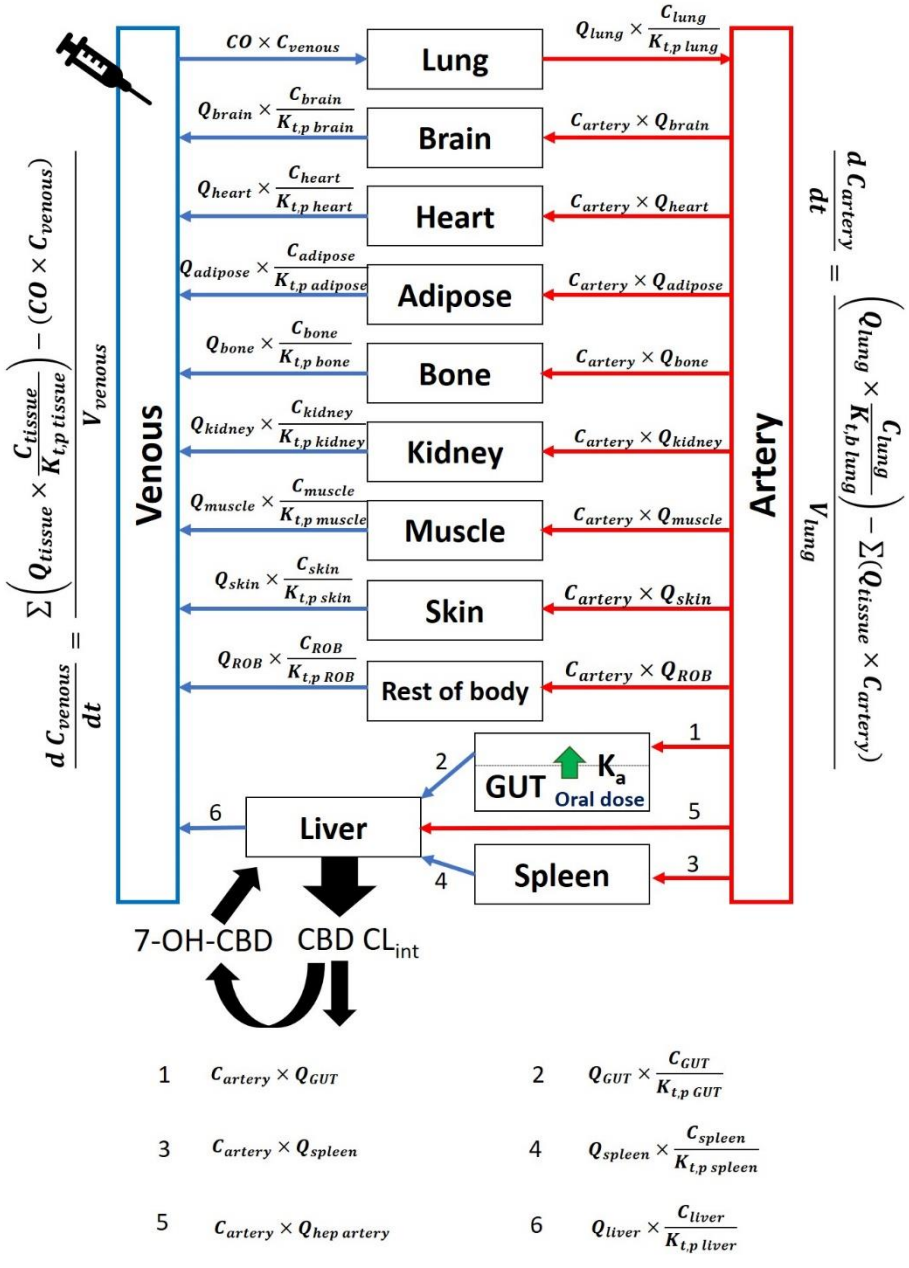

Figure 2. *Structure of the whole-body PBPK model for CBD and 7-OH-CBD. The body was divided into 12 compartments connected by venous and arterial blood flows.*

The tissue distribution was described by a set of the ordinal differential equation (ODE) under assumption of perfusion-limitation with homogenous rapid tissue distribution as follows:

Non-eliminating tissues (except the lungs):

$$\frac{d\,C_{tissue}}{dt} = \frac{Q_{tissue} \times (C_{artery} - C_{tissue} \times \frac{BP}{K_{t,p\ tissue}})}{V_{tissue}}$$

Lungs:

$$\frac{d\,C_{lung}}{dt} = \frac{(CO \times C_{venous}) - (Q_{lung} \times C_{lung} \times \frac{BP}{K_{t,p\ lung}})}{V_{lung}}$$

Venous blood:

$$\frac{d\,C_{venous}}{dt} = \frac{\Sigma\left(Q_{tissue,i} \times C_{tissue,i} \times \frac{BP}{K_{t,p,i}}\right) - (CO \times C_{venous})}{V_{venous}}$$

Arterial blood:

$$\frac{d\,C_{artery}}{dt} = \frac{\left(Q_{lung} \times C_{lung} \times \frac{BP}{K_{t,p\ lung}}\right) - \Sigma\left(Q_{tissue\ i} \times C_{artery}\right)}{V_{artery}}$$

Liver (eliminating tissue):

$$\frac{d\,C_{liver}}{dt} = \frac{\begin{array}{c}(Q_{hepartery} \times C_{artery}) + (Q_{GUT} \times C_{GUT} \times \frac{BP}{K_{t,p\ GUT}}) + (Q_{spleen} \times C_{spleen} \times \frac{BP}{K_{t,p\ spleen}}) \\ -(Q_{liver} \times C_{liver} \times \frac{BP}{K_{t,p\ liver}}) - (C_{u,liver} \times CL_{int})\end{array}}{V_{liver}}$$

3.5.2 PARAMETERIZATION OF TISSUE VOLUMES, TISSUE BLOOD FLOWS, INTRINSIC CLEARANCE, AND TISSUE-TO-PLASMA PARTITION COEFFICIENTS

The tissue volumes and blood flows were obtained from the literature (111-113). The *in vivo* hepatic CL_{int} was scaled from *in vitro* hepatic CL_{int} (obtained from the experiment section 3.3) using milligram microsomal protein per gram liver (MPPGL) and liver weight, both calculated as follows:

Milligram microsomal protein per gram liver (adults and children) (114):

$$\mathrm{MPPGL} = 10^{1.407+0.0158\times\mathrm{age}-0.00038\times\mathrm{age}^2+0.0000024\times\mathrm{age}^3}$$

Lean liver weight in adults (based on lean bodyweight) (115, 116):

$$\mathrm{LLW\ (g)} = (0.36 + 0.023 \times \mathrm{LBW}) \times 1000$$

$$\mathrm{LBW\ (kg)} = \frac{9270 \times \mathrm{BW}}{(6680 + 216 \times \mathrm{BMI})}$$

Liver weight in children (117):

$$\mathrm{LW\ (g)} = 0.0072 \times \mathrm{age}^5 - 0.3975 \times \mathrm{age}^4 + 7.9052 \times \mathrm{age}^3 - 65.624 \times \mathrm{age}^2 + 262.02 \times \mathrm{age} + 157.52$$

The tissue-to-plasma partition coefficient ($K_{t,p}$) were estimated by the formula suggested by Poulin and Theil using values for tissue compositions, octanol-water partition coefficient (P), plasma unbound fraction ($f_{u,p}$), and tissue unbound fraction ($f_{u,t}$) as follows (118):

$$\mathrm{K_{t,p}} = \frac{\mathrm{P} \times \left(\mathrm{f_{nl,t}} + 0.3\mathrm{f_{ph,t}}\right) + \left(\mathrm{f_{w,t}} + 0.7\mathrm{f_{ph,t}}\right)}{\mathrm{P} \times \left(\mathrm{f_{nl,p}} + 0.3\mathrm{f_{ph,p}}\right) + \left(\mathrm{f_{w,p}} + 0.7\mathrm{f_{ph,p}}\right)} \times \frac{\mathrm{f_{u,p}}}{\mathrm{f_{u,t}}}$$

where f_{nl}, and f_{ph} are respectively fractions of neutral lipid and phospholipid. The partition coefficient of $10^{6.3}$ (logP = 6.3) and $10^{5.94}$ (log P = 5.94) for CBD and 7-OH-CBD, respectively, were used for estimation. The plasma unbound fraction for both compounds were set equally at 0.1 (75, 76). For adipose tissue, the value of P was replaced by an olive oil-water partition ratio (D) which was calculated as (119):

$$\mathrm{D} = 10^{1.115 \times \mathrm{logP} - 1.35}$$

The tissue unbound fraction ($f_{u,t}$) was estimated from the $f_{u,p}$ value as:

$$f_{u,t} = \frac{1}{1 + \frac{1 - f_{u,p}}{f_{u,p}} \times R}$$

where R is a fixed value of either 0.5 or 0.15 for lean and adipose tissues, respectively (120).

The pediatric $f_{u,p}$ value was corrected by albumin blood concentrations varying by age as follows (111, 121):

$$f_{u,pediatric} = \frac{1}{1 + \frac{(1 - f_{u,adult}) \times albumin_{pediatric}}{f_{u,adult} \times albumin_{adult}}}$$

$$albumin_{pediatric}(g/L) = 33.746 + 1.1287 \times \log(365 \times age)$$

3.5.3 CLINICAL DATA FOR MODEL VALIDATION

In adults, clinical data in healthy subjects receiving CBD alone were selected. One clinical study with intravenous (73) and six clinical studies with oral administration (62, 75, 76, 122-124) were used for model validation. Two clinical pharmacokinetic pediatric studies identified were employed for model validation. The study by Devinsky *et al*. included children aged 4-11 years of age, diagnosed with Dravet syndrome, who received escalating CBD doses (Epidiolex®), starting from 2.5 mg/kg/day with titration up to 20 mg/kg/day in combination with antiseizure medications including valproic acid, clobazam, levetiracetam, topiramate and stiripentol (125). The second study conducted by Wheless *et al*. involved children diagnosed with treatment-resistant epilepsy in the age range of 1–18 years who received the synthetic pharmaceutical-grade CBD in combination with antiseizure medications without non-CYP450 inducing or inhibiting properties (126).

3.5.4 PBPK MODEL DEVELOPMENT

For comparison with clinical data, the pediatric PBPK model was simulated based on the same input parameters as reported in the clinical studies specifically bodyweight, height, age, dose, and dosing interval. Identical to

adult model absorption rate constants (K_a), gastrointestinal transit time (tr) in terms of the first-order transit rate constant (K_{tr}) as $\frac{1}{tr}$, and dose-dependent fraction absorbed through GUT tissue (F_{abs}) were applied for pediatric model.

3.5.5 EVALUATION OF MODEL PERFORMANCE

Model validation was performed by comparing the predicted concentration-time profiles, areas under the concentration-time curve (AUC), maximum concentration (C_{max}) and/or trough concentration (C_{trough}) to the corresponding clinical observations. Predictions within a 2-fold boundary (0.5-2.0 fold difference) around the observation was considered as medium to moderate accuracy (127).

3.5.6 MODEL APPLICATIONS

The pediatric model was applied for predicting recommended doses resulting in steady-state trough concentrations ($C_{ss,trough}$) of 100 ng/mL, previously reported as an effective concentration (128) in children.

4 RESULTS

4.1 BIOANALYTICAL METHOD DEVELOPMENT (PAPER I)

4.1.1 COMPOUND SPECIFIC PARAMETERS FOR MASS SPECTROMETRY

The negative ionization mode provided a superior signal-to-noise response for all analytes and was selected for further analysis (**Figure 3**). The quantifier and qualifier transitions of all analytes are summarized in **Table 1**. The ion spray voltage and temperature were optimized to -3000 volts and 100°C, respectively. The response was recorded in multiple reaction monitoring (MRM) mode.

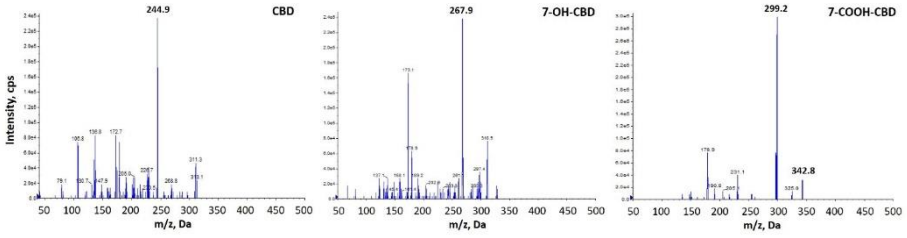

Figure 3. *Fragmentation patterns when applying the selected collision energies to the analytes: CBD: -38 V, 7-OH-CBD: 35 V, and 7-COOH-CBD: -25 V. The signals were recorded in negative ionization mode.*

Table 1. *Summary of information of all analytes including quantifier and qualifier transitions.*

Parameter	(-)-CBD	(-)-7-OH-CBD	(-)-7-COOH-CBD
Molecular weight	314.47	330.46	344.44
Q1 (*m/z*)	313.00	329.00	343.00
Quantifier transition (Q3) (*m/z*)	245.00	268.00	299.00
Qualifier transition (Q3) (*m/z*)	255.00	261.00	255.00
DP (volt)	-90	-80	-80
EP (volt)	-5	-5	-5
CE (volt)	-38	-35	-25
EXP (volt)	-20	-20	-20

4.1.2 CHROMATOGRAPHIC CONDITIONS

A 50 × 4.6 mm C-18 BDS Hypersil column, particle size 3 µm (Thermo Scientific) completely and rapidly separated all the analytes within 3.5 minutes using an isocratic mobile phase consisting of 0.4 mM ammonium acetate and acetonitrile (15:85 v/v) at a flow rate of 0.4 mL/min. The retention times were 2.7 1.7, and 1.4 minutes for CBD, 7-OH-CBD, and 7-COOH-CBD respectively (**Figure 4**). The elution times were approximately 2-fold increased to 4.9, 3.3, and 2.8 minutes, respectively, when a longer 100 × 4.6 mm column was utilized (**Figure 5**).

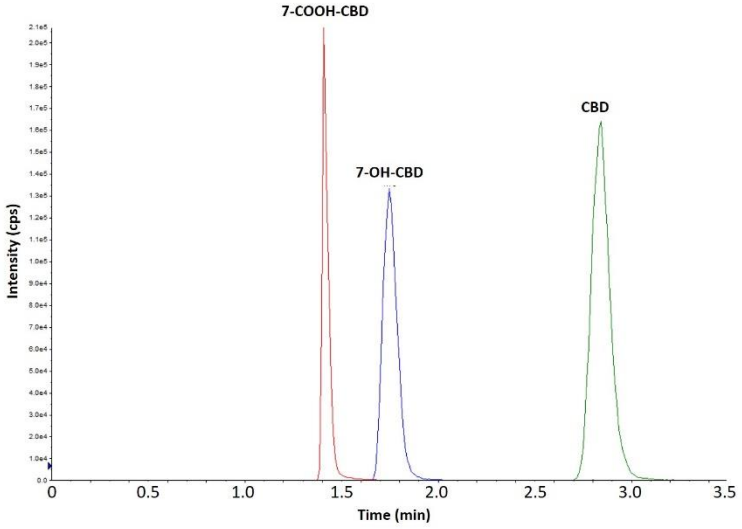

Figure 4. *Chromatograms demonstrating a rapid separation of CBD, 7-OH-CBD, and 7-COOH-CBD in a 50 ×4.6 mm C-18 BDS Hypersil column (particle size 3 µm) with isocratic elution using a mixture of 0.4 mM ammonium acetate and acetonitrile (15:85 v/v) at a flow rate of 0.4 mL/min.*

4.1.3 VALIDATION

Simple protein precipitation using an equal volume of acetonitrile was sufficient to extract the analytes with a recovery above 65% for all analytes.

The responses, expressed as peak-area ratio to the internal standard, of CBD and 7-COOH-CBD correlated linearly to the corresponding concentrations with a coefficient $R > 0.99$ using $1/Y^2$ weighting factor, while 7-OH-CBD was

best fitted to a quadratic function also with $1/Y^2$ weighting. The precision and accuracy tests were within the acceptable ranges. With an injection volume of 10 µL, the lower limit of quantitation (LLOQ) was 5 nM for CBD and 7-OH-CBD, while it was 50 nM was for 7-COOH-CBD. The method showed acceptable sensitivity and selectivity. None of the tested antiseizure medications interfered chromatographically with CBD or its two main metabolites.

When using a 50 50 × 4.6 mm C-18 BDS Hypersil column, Δ9-THC and 11-COOH-THC were co-eluted at the same retention times as CBD and 7-COOH-CBD, respectively. However, these compounds could be separated using the longer column, 100 × 4.6 mm C-18 BDS Hypersil (**Figure 5**).

CBD and the two metabolites were generally stable at -30°C and during five freeze-thaw cycles. However, at refrigerated temperature for two months, 7-COOH-CBD in plasma was more prone to degradation, with concentrations reduced by >15%.

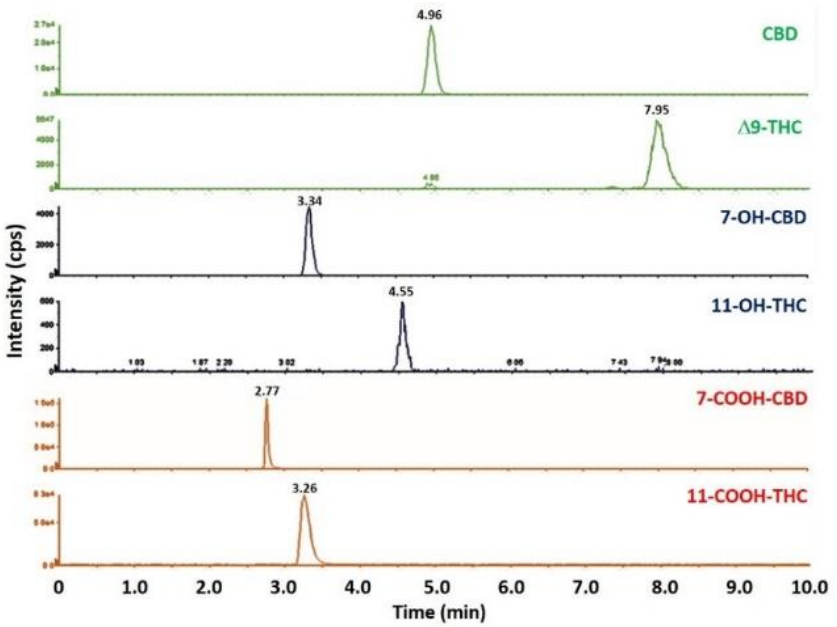

Figure 5. *Chromatograms demonstrating separation of CBD, 7-OH-CBD, 7-COOH-CBD, Δ9-THC, 11-OH-THC, and 11-COOH-THC in a 100 × 4.6 mm C-18 BDS Hypersil column (paricle size 3 µm) under isocratic elution using a mobile phase of 0.4 mM ammonium acetate and acetonitrile (15:85 v/v) at flow rate of 0.4 mL/min.*

4.2 EVALUATION OF THE IMPACT OF ANTI-SEIZURE MEDICATIONS AND MODERATE-ACTIVITY CYP2C19 GENOTYPES ON CBD METABOLISM (PAPER II)

Initial *in vitro* CBD depletion rate constants (k_{init}) were concentration-dependent (**Table 2**). A Michaelis-Menten model fitted to the obtained initial depletion rates in the control group (CBD alone) yielded V_{max} and K_m estimates of 2.16 nmol/min/nmol CYP450 and 422 nM, respectively, corresponding to an *in vitro* CL_{int} value of 5.12 mL/min/nmol CYP450. Co-incubated antiseizure medications (valproic acid, clobazam, stiripentol and topiramate) resulted in diminished CBD depletion rates, with the highest reduction observed in a combination with four antiseizure medications. The estimated V_{max} values for incubation in which antiseizure medications were co-incubated with CBD were approximately comparable, except for the combination with four antiseizure medications that was even more reduced (**Figure 6A** and **7**), whereas the K_m values increased in all combined conditions. This resulted in decreased *in vitro* CL_{int} values, however, the predicted hepatic clearance was not largely affected (**Figure 7**).

Moderate-activity CYP2C19 showed a slightly increased K_m value that did not markedly reduce CBD *in vitro* CL_{int} (3.59 mL/min/nmol CYP450). *In vitro-in vivo* extrapolation predicted an increased CBD unbound concentration by 1.3- to 4.8-fold for the tested combinations.

The formation rate of the active metabolite 7-OH-CBD was proportional to the CBD initial concentration, and tended to be negligibly or minimally reduced when CBD was co-incubated with 1-3 ASMs, but became markedly decreased in a combination with four antiseizure medications (**Figure 6B**).

The combination of CBD with valproic acid, clobazam, and topiramate did not influence 7-COOH-CBD formation rate, while combinations including stiripentol highly reduced the formation of this metabolite (**Figure 6C**).

***Table 2**. Initial in vitro depletion rate constants (k_{init}) observed for various concentrations of CBD in human liver microsome incubation mixtures containing 0.0377 nmol CYP450/mL. Values are presented in min^{-1}.*

CBD concentration (nM)	Control	VPA+CLB	STP	TPM	3ASMs	4ASMs
400	0.086	0.074	0.076	0.079	0.058	0.025
600	0.077	0.050	0.067	0.057	0.040	0.017
800	0.062	0.045	0.044	0.055	0.042	0.025
1000	0.068	0.045	0.046	0.053	0.040	0.016
2000	0.035	0.028	0.030	0.036	0.017	0.013
4000	0.020	0.018	0.014	0.015	0.015	0.006
6000	0.011	0.010	NA	0.011	0.010	NA

VPA: valproic acid, CLB: clobazam, STP: stiripentol, TPM: topiramate, 3ASMs: VPA+CLB+STP, 4ASM: VPA+CLB+STP+TPM.
NA: not available due to lack of trend

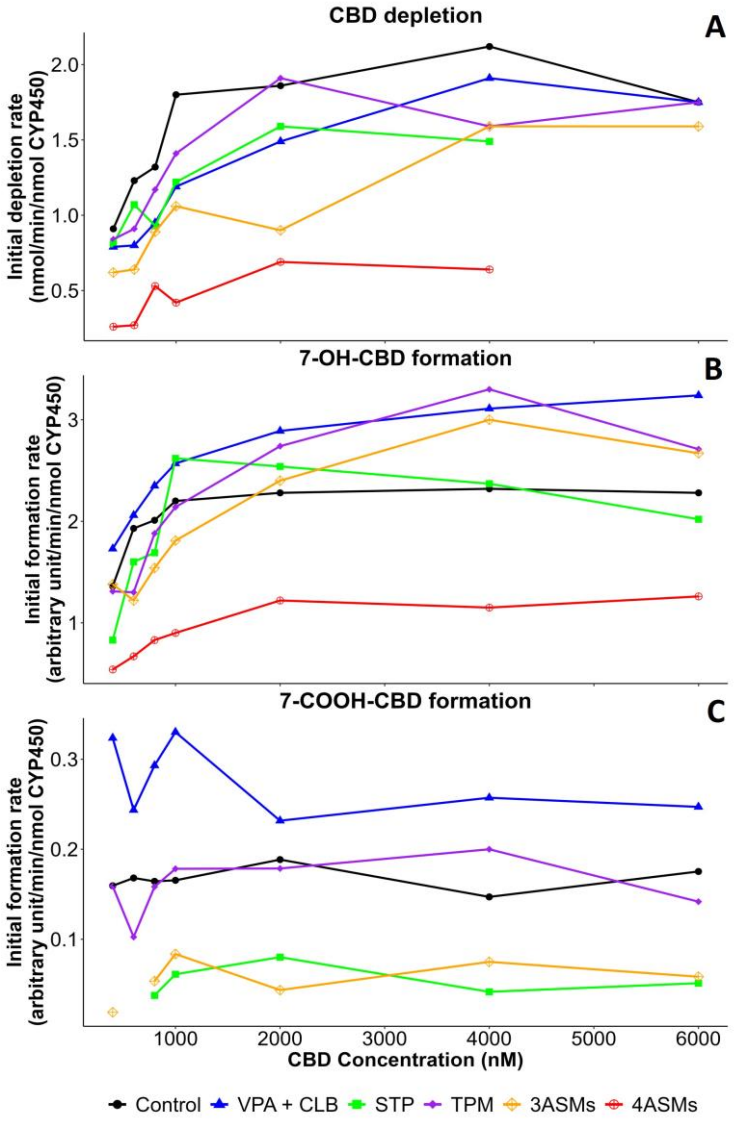

Figure 6. *CBD initial depletion rate (A), 7-OH-CBD formation rate (B), and 7-COOH-CBD formation rate (C) at various initial CBD concentrations (x-axis) in pooled human liver microsomes when combined with different antiseizure medications. Data of the control group was presented as median value from three independent experiments, while those of the other combinations were obtained from one single experiment. A marked reduction of CBD depletion rate and 7-OH-CBD formation rate were observed in a combination with four ASMs. A marked reduction of 7-COOH-CBD formation rate was observed in a combination consisting of STP. VPA: valproic acid, CLB: clobazam, STP: stiripentol, TPM: topiramate, 3ASMs: VPA+CLB+STP, 4ASM: VPA+CLB+STP+TPM.*

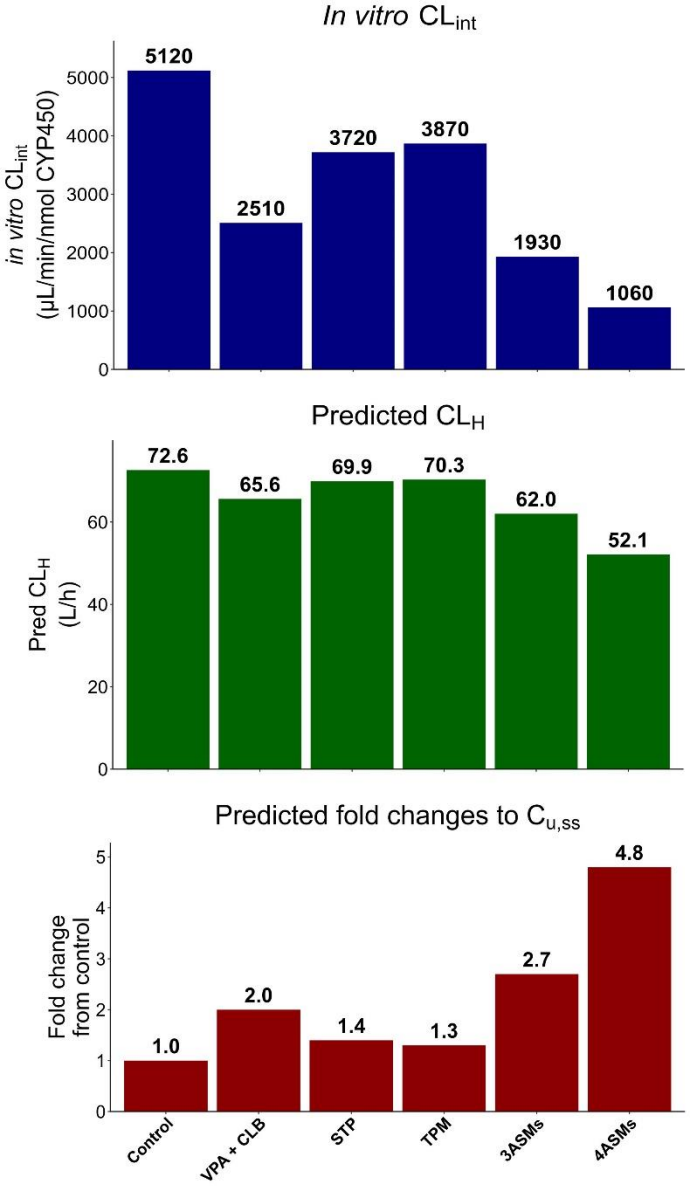

Figure 7. *CBD in vitro CL_{int} values (upper panel) when incubated alone and when combined with antiseizure medications (ASMs) in pooled human liver microsomes. Middle panel: predicted hepatic clearances scaled from in vitro results. Bottom panel: predicted fold changes in steady-state CBD unbound concentrations. Data of the control group is presented as median value from three independent experiments, while those of the other combinations were obtained from one single experiment. VPA: valproic acid, CLB: clobazam, STP: stiripentol, TPM: topiramate, 3ASMs: VPA+CLB+STP, 4ASM: VPA+CLB+STP+TPM.*

4.3 EVALUATION OF POTENTIAL IMPACT OF ANTISEIZURE MEDICATION CYP3A4 SUBSTRATES ON METABOLISM OF CBD AND 7-OH-CBD (PAPER III)

The depletion rate constant (k) of CBD incubated alone with HLMs was 0.132 min^{-1} corresponding to a half-life and $CL_{int,vt}$ of 5.26 minutes and 2240 µL/min/nmol CYP450, respectively. Combinations with other antiseizure medications, except stiripentol, minimally reduced CBD *in vitro* CL_{int} to 1840-2070 µL/min/nmol CYP450 (9-18%), whereas stiripentol markedly decreased CBD $CL_{int,vt}$ to 730 µL/min/nmol CYP450 (~65%). A combination with four antiseizure medications metabolized by CYP3A4 (zonisamide, felbamate, ethosuximide and perampanel) marginally decreased CBD *in vitro* CL_{int} to 1950 µL/min/nmol CYP450 (~13%). It was predicted from the reduced CL_{int} values that unbound concentrations of CBD at steady state ($C_{u,ss}$) would marginally increase by 1.2 fold, except the combination with stiripentol that could lead to a 3-fold increase in CBD $C_{u,ss}$ (**Figure 8**).

With the exception of stiripentol, co-incubateion with antiseizure medications did not affect the initial formation rate of 7-OH-CBD which ranged 0.033-0.050 arbitrary unit/min/nmol CYP450. The rate reduced to 0.004 arbitrary unit/min/nmol CYP450 in the presence of stiripentol. The depletion rate of this metabolite, when CBD alone was incubated with HLMs, was 0.041 min^{-1} corresponding to a CL_{int} of 690 µL/min/nmol CYP450. Unlike CBD, a combination with other antiseizure medications markedly reduced the metabolism of this metabolite to 420-460 (34-39%) µL/min/nmol CYP450, with an even greater reduction to 370 µL/min/nmol CYP450 (~46%) in a combination with four antiseizure medications metabolized by CYP3A4. 7-OH-CBD $C_{u,ss}$ was predicted to increase by 50-90%, with the highest increase by around 90% in a combination with four antiseizure medications CYP3A4 substrates (**Figure 9**).

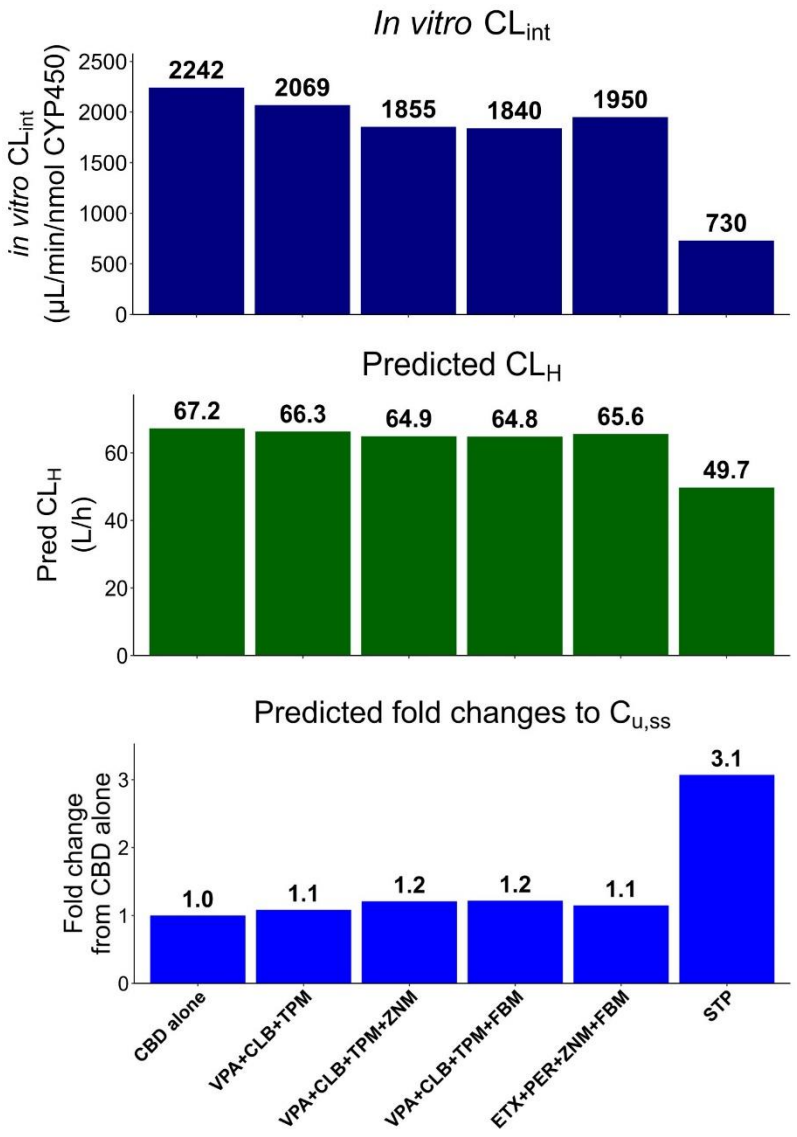

Figure 8. *CBD in vitro CL_{int} values (upper panel) when incubated alone and when combined with antiseizure medications (ASMs) in pooled human liver microsomes. Middle panel: predicted hepatic clearances scaled from in vitro results. Bottom panel: predicted fold changes in steady-state CBD unbound concentrations. STP markedly decrease CBD metabolism, whereas ASMs competing CYP3A4 enzyme (ETX, PER, ZNM, FBM) marginally affected this process. Data is presented as median value from three independent experiments all conditions, except for the combination CBD+ETX+PER+ZNM+PBM which was performed in duplicate wherefor the value is averaged. VPA: valproic acid, CLB: clobazam, STP: stiripentol, TPM: topiramate, ZNM: zonisamide, FBM: felbamate, ETX: ethosuximide, PER: perampanel.*

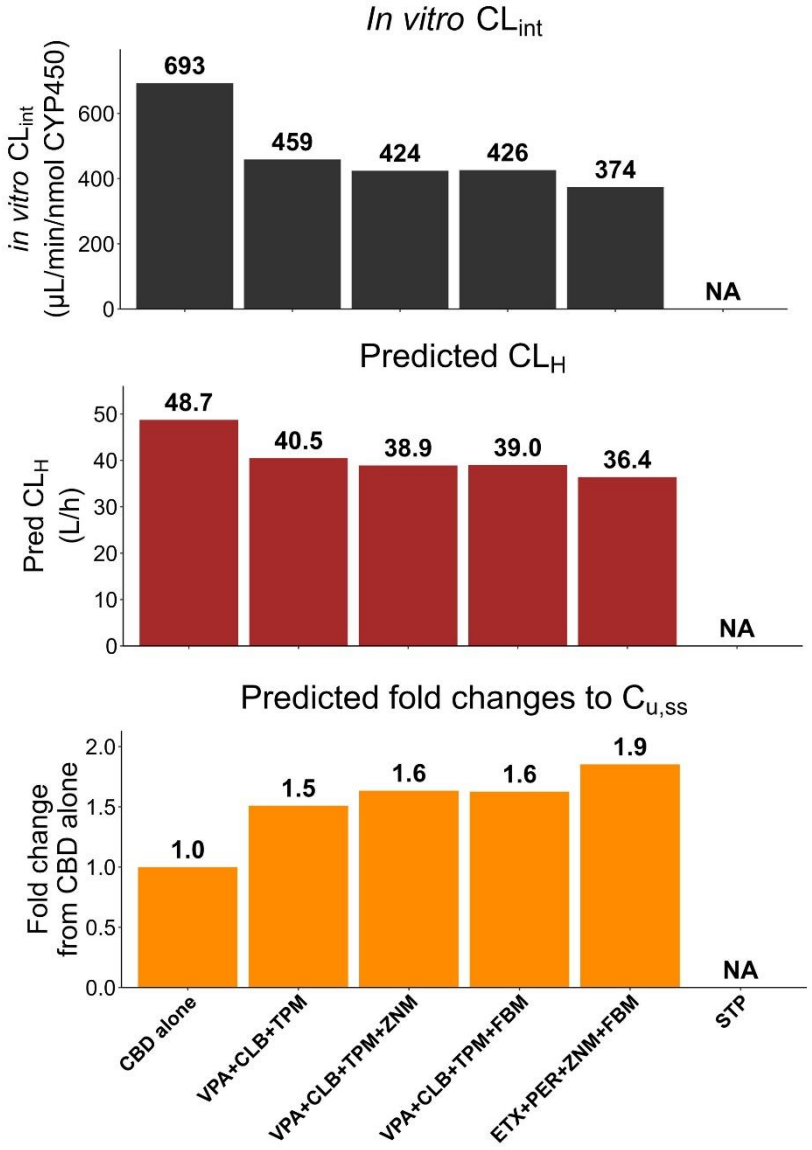

Figure 9. *7-OH-CBD in vitro CL_{int} values (upper panel) when CBD was incubated alone and when combined with antiseizure medications (ASMs) in pooled human liver microsomes. Middle panel: predicted hepatic clearances scaled from in vitro results. Bottom panel: predicted fold changes in steady-state CBD unbound concentrations. STP markedly decrease CBD metabolism, whereas ASMs competing CYP3A4 enzyme (ETX, PER, ZNM, FBM) marginally affected this process. Data is presented as median value from three independent experiments. VPA: valproic acid, CLB: clobazam, STP: stiripentol, TPM: topiramate, ZNM: zonisamide, FBM: felbamate, ETX: ethosuximide, PER: perampanel. NA: not available due to no established formation slope.*

4.4 PHARMACODYNAMIC EVALUATION OF CBD IN HUMAN IPSC-DERIVED 3D NEURAL MODEL OF ACUTE SEIZURE ACTIVITY (PAPER IV)

4.4.1 ESTABLISHMENT OF SEIZURE-LIKE ACTIVITY

Seizure-like activity was successfully established in cultured human iPSC-derived neuronal networks using two acute pharmacological models. Two models provided distinct electrophysiological signatures. Application of 4-aminopyridine (4-AP) enhanced neuronal excitability, increasing the occurrence of network bursts and the proportion of spikes occurring within bursts, and produced relatively regular bursting rhythms. In contrast, Mg^{2+}-free conditions induced more pronounced alterations in bursting characteristics, including longer burst duration, increased burst spike count and spike rate, reduced inter-burst spiking, and the appearance of population superbursts with irregular rhythmicity.

4.4.2 EFFICACY AND POTENCY OF CBD

CBD produced concentration- and time-dependent suppression of seizure-like activity in both models. Minimal effects were observed at 1 µM, whereas concentrations of 5–10 µM markedly reduced spike rate, network burst frequency, and burst duration, with significant suppression generally evident after approximately 20 minutes of exposure. At 40–60 minutes, CBD at 10 µM produced greater than 75% reduction of network bursting in the 4-AP model and comparable inhibition in the Mg^{2+}-free model. Estimated EC_{50} values for most electrophysiological parameters ranged between 2 and 10 µM, with particularly strong sensitivity observed for network burst counts (approximately 2–4 µM).

4.4.3 NEURONAL ACTIVITY AFTER CBD EXPOSURE

Washout experiments demonstrated that CBD-induced suppression at 10 µM was reversible, with neuronal activity recovering after replacement with fresh medium. In contrast, exposure to 100 µM CBD caused persistent loss of neuronal activity that did not recover even after prolonged washout, indicating concentration-dependent neurotoxicity at high doses.

4.5 DEVELOPMENT OF A PHYSIOLOGICALLY-BASED PHARMACOKINETIC MODEL FOR CANNABIDIOL (PAPER V)

The PBPK model for CBD was first developed for adults based on seven clinical studies in healthy subjects who received either intravenous or oral administration of CBD. Simulation of intravenous administration (73) showed a good prediction of the area under the concentration-time curve ($AUC_{0-\infty}$ or $AUC_{0-\tau}$), systemic clearance (CL) and volume of distribution (V_z) within a 2-fold boundary around the observations. In the oral model, the predicted maximum concentration (C_{max}), AUCs, CL/F and V_z/F values agreed fairly with the clinical reports (62, 75, 76, 122, 124), while underprediction was observed for simulations for one clinical study (123). The model predictions for intravenous administration were sensitive to an increased hepatic blood flow, while the oral model was influenced by changes in intrinsic hepatic clearance and plasma unbound fraction. The model predicted an CBD hepatic extraction ratio of approximately 0.85.

The pediatric model was consequently developed from the adult model using the same parameters describing absorption processes including absorption rate constants, gastrointestinal transit times and dose-dependent fraction absorbed (F_{abs}). Model predictions compared to two available clinical pediatric studies with pharmacokinetic information showed that predicted values for $AUC_{0-\tau}$, CL and V_z generally lied within a 2-fold boundary around the observations. The model performed well when simulating the study by Wheless *et al.* (126), with the exception of infants one year of age for whom plasma concentrations were overpredicted. With some exceptions, the model adequately predicted exposures (AUCs) and concentration-time results reported by Devinsky *et al.* (125).

The developed PBPK model suggested higher doses per bodyweight in younger children with a tendency to decrease with age in order to achieve the same steady state trough concentration. As expected, the predicted doses reflected age-dependent values of plasma unbound fraction, hepatic intrinsic clearance and the fraction absorbed combined (**Figure 10**).

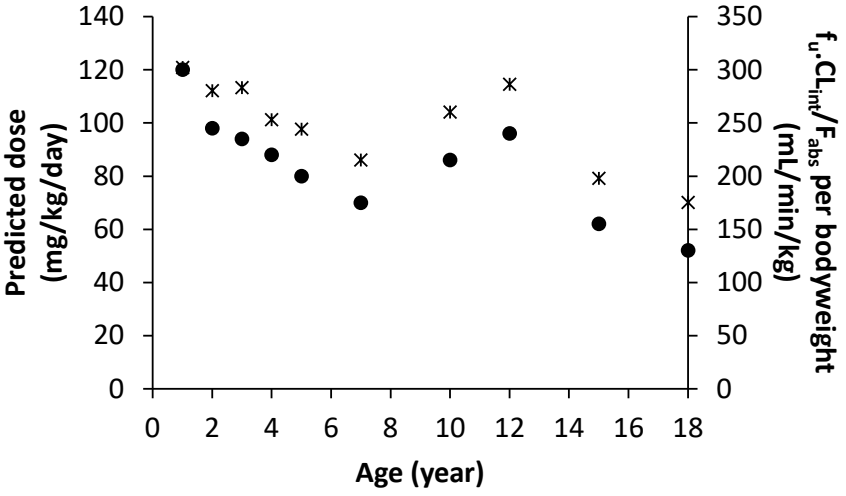

Figure 10. *Model predicted CBD doses resulting in a steady state trough concentration of 100 ng/mL in children of varying ages when administered alone twice daily. The predicted doses (●) reflected age-dependent values of plasma unbound fraction (f_u), hepatic intrinsic clearance (CL_{int}), and fraction absorbed (F_{abs}) combined ($\frac{f_u \times CL_{int}}{F_{abs}}$) (*).*

5 DISCUSSION

5.1 BIOANALYTICAL METHOD DEVELOPMENT (PAPER I)

The simple but sensitive bioanalytical for quantifying CBD, 7-OH-CBD and 7-COOH-CBD in plasma was successfully developed and validated. Although several HPLC-MS/MS assays for CBD are already available in the literature, some involve complicated procedures. The proposed method offers a simplified workflow, including straightforward sample preparation and analysis procedures.

The negative ionization mode applied for all analytes together with isocratic elution resulted in a rapid sample turnover within 3.5 minutes when using the 50 × 4.6 mm C-18 column (BDS Hypersil, particle size 3 µm, Thermo Scientific). In the presence of THC, co-elution of CBD/THC and 7-COOH-CBD/11-COOH-THC could be solved by using a qualifier transition or utilizing the longer column (100 × 4.6 mm C-18 column. The result from this work provides two optional methods to quantify CBD and the metabolites depending on whether THC and its metabolites are present.

The calibration curve range covered the expected plasma concentration for all analytes following CBD clinical doses as reported in clinical studies. The attainment of accuracy and precision criteria suggested that the method is able to reliably and effectively analyze these compounds in plasma samples.

Further, this developed method was demonstrably applied for analysis of these compounds in other aqueous matrices as demonstrated in Papers II and III.

5.2 EVALUATION OF THE IMPACT OF ANTI-SEIZURE MEDICATIONS AND MODERATE-ACTIVITY CYP2C19 GENOTYPES ON CBD METABOLISM (PAPER II)

Hepatic intrinsic clearance is a key factor determining CBD exposure *in vivo*. This experiment used the Michaelis-Menten model to estimate an intrinsic metabolic clearance using maximal reaction velocity (V_{max}) and the Michaelis-

Menten constant (K_m). From the experiment, the depletion rate constant (k) was found to be concentration-dependent. This value tended to diminish with increasing CBD concentrations, implying saturation kinetics.

The impacts of antiseizure medication with different CYP450-inhibitory effects as well as those which are not CYP450 substrates were investigated, such as valproic acid (CYP2C9 inhibitor), stiripentol (strongly CYP3A4 and CYP2C19 inhibitor), clobazam (CYP3A4 substrate) and levetiracetam (non-CYP450 substrate). The changes in CBD hepatic intrinsic clearances varied depending on the co-incubated antiseizure medications. Those antiseizure medications being non-CYP450 substrates did not affect CBD hepatic intrinsic clearance, meaning that antiseizure medications renally excreted or metabolized by non-CYP450 pathway are unlike to increase CBD exposure *in vivo*.

HLMs from moderate-activity CYP2C19 genotypes did not demonstrate a marked reduction of CBD metabolism, suggesting that CBD dose adjustment may not be required for heterogenous CYP2C19 genotype.

5.3 EVALUATION OF POTENTIAL IMPACT OF ANTISEIZURE MEDICATION CYP3A4 SUBSTRATES ON METABOLISM OF CBD AND 7-OH-CBD (PAPER III)

This experiment was extended from the previous drug metabolic study but now focusing on the role of CYP3A4 which has been reported as the major enzyme metabolizing CBD in human liver microsomes (106). The experiment design was different from the previous study as only one concentration of CBD (100 nM) was used. In addition, the metabolic profile of CBD's active metabolite 7-OH-CBD was also examined. Further, additional antiseizure medication CYP3A4 substrates were included.

The experiment revealed that CBD and 7-OH-CBD metabolism occurs mainly through the CYP3A4 pathway. CBD is at the same time metabolized by CYP2C19 pathway by which the active metabolite 7-OH-CBD is mainly formed. Any antiseizure medication that strongly inhibits these two enzymes could significantly decrease CBD metabolism, resulting in its higher exposure.

This could be an approach to improve clinical efficacy as elevated oral doses do not increase systemic exposure in a proportional manner.

As CYP2C19 pathway is essential for 7-OH-CBD formation, inhibition of this enzyme would at the same time result in a reduction of the exposure of this metabolite as observed from the effect of stiripentol. Unlike stiripentol, antiseizure medication CYP3A4 substrates minimally affected CBD metabolism, but they showed a high impact on 7-OH-CBD metabolism. These *in vitro* results highlight the different roles of CYP3A4 inhibitors and CYP3A4 substrates, respectively, to manage the exposure to CBD and its active metabolite, but also provide preliminary information on selecting combination regimens in which CBD is included.

Since newer generation antiseizure medications generally do not have CYP450 inhibiting properties, co-medication with CBD may not be able to much reduce *in vivo* CBD metabolism. Dose optimization is challenging for at the same time regulating the exposure of both CBD and 7-OH-CBD. Stiripentol could be a possible antiseizure compound to be co-administered with CBD if increased systemic exposure to the latter is desired.

5.4 PHARMACODYNAMIC EVALUATION OF CBD IN HUMAN IPSC-DERIVED 3D NEURAL MODEL OF ACUTE SEIZURE ACTIVITY (PAPER IV)

This study investigated the pharmacodynamic properties of CBD in terms of efficacy, potency as well as neurotoxicity in human iPSC-derive neural culture model of acute seizure activity coupled with the use of multi-electrode array (MEA) recordings. The results revealed a robust and reproducible CBD effect on electrophysiological function, and were consistent with those observed in rodent hippocampal slices (54). This could suggest a potential to replace the use of brain slices. In addition, MEA recordings is more advantageous than patch cramp technique as it enables an assessment of electrophysiological function of both single neuron and neuronal network. Importantly, the use of human iPSC-derived neurons revealed the toxic concentrations that does not become obvious when using the brain slice preparations.

Both 4-AP and Mg^{2+}-free models have been employed for investigation of electrophysiological function in neurons for decades. Many currently used antiseizure medications were proved for their antiseizure activity by these models (88, 90). The ability of the model to capture CBD effects suggested a potential antiseizure effect of CBD. Further, a lower EC_{50} value of CBD compared with other antiseizure medications (88), could imply CBD being more potent.

Although 4-AP blockage and Mg^{2+}-free conditions are not exactly identical to the events occurring in the brain, some clinically relevant features of these models (95, 96, 102) could reliably imply the *in vitro* results to clinical situations.

CBD exhibited both concentration- and time-dependent effects *in vitro*, suggesting that optimal amount of time are required for CBD to exert the full clinical antiseizure activity. The obtained neurotoxic information is also important to be considered. Increasing CBD dosing may be expected to result in brain concentrations exceeding neurotoxic concentrations thus possibly causing side effects.

5.5 DEVELOPMENT OF A PHYSIOLOGICALLY-BASED PHARMACOKINETIC MODEL FOR CANNABIDIOL (PAPER V)

The whole PBPK model for CBD and 7-OH-CBD was developed bottom-up using literature data and in-house *in vitro* experiment to determine clearance. Perfusion limited disposition kinetics was assumed for CBD due to its high lipophilicity. The model was first developed based on clinical data in adults and was then extended to include a pediatric population.

In the model for adults, a good predictive capability for intravenous administration suggested that the model adequately described CBD disposition although overprediction was observed in the late distribution phase. For oral administration, absorption makes the model more complex. Defining the absorption rate constant (K_a) is challenging since no conclusive information was available. Four publications reported different K_a values. Of these, three articles reported the first-order K_a values ranging from 0.0048-0.0153 min^{-1} (61, 129, 130), whereas the fourth described CBD rate of absorption by a

Weibull function (67). The K_a value used in the present PBPK model was obtain by feathering of clinical data (method of residuals) (75).

In the present model, CBD absorption was assumed to take place from duodenum until ascending colon, with negligible absorption in duodenum and jejunum but extensive absorption in ileum and ascending colon. The K_a values for these upper small intestinal segments were therefore set to zero. Although this is not physiologically realistic since absorption also occurs in the upper small intestine, simulation provided the best agreement with clinical median time to C_{max} value (T_{max}) observed at 4-5 hours following oral administration. The delayed T_{max} may be explained by the low water solubility of CBD with a tendency to precipitate at the low pH in the stomach (131). The redissolution of the precipitates would result in a delayed absorption.

The lower predictions observed for a single oral dose for some clinical studies as well as at steady state after multiple dosing could be explained by a too high intrinsic clearance value obtained from the *in vitro* investigation in human liver microsomes. Simulation in this thesis was performed based on a normal condition without substrate auto-inhibition which has been reported as a property of CBD (129). Further, an underprediction observed for the pediatric model may be due to an exclusion of drug-drug interactions from simulations, even though all pediatric study subjects received antiseizure medications combined with CBD. Some medications were those shown to reduce CBD intrinsic clearance in this thesis (Papers II and III). The observed pharmacokinetic parameters reported in pediatric clinical study by Devinsky *et al*. (125) were estimated based on only three plasma concentration time-points. This may lead to an imprecise comparison with simulated values.

Two PBPK models have previously been developed for CBD using Simcyp® software, whereas the PBPK model in this thesis was developed using Berkeley Madonna which is an open platform being flexible to modifications in the written script for further simulations of varying conditions.

Overall, thesis developed a useful PBPK model based on clinical studies with satisfactorily predictive capacity for pharmacokinetic parameters of CBD. Together with information on drug-drug interactions as well as the preliminary EC_{50} values in the cultured human iPSC-derived neurons, an extended PBPK model could potentially predict the optimal recommended doses yielding desired exposure.

6 CONCLUSIONS

This thesis presents new knowledge on the metabolism of CBD and its active metabolite 7-OH-CBD aiming to provide information for regulating *in vivo* CBD exposure, as well as optimizing CBD clinical dose in both children and adults.

The bioanalytical method developed for quantifying CBD and main metabolites 7-OH-CBD and 7-COOH-CBD in plasma meets validation criteria according to FDA recommendations. The method involves simple procedures and rapidly quantifies all analytes in one single run with eluting time within 3.5 minutes. The developed method covers the expected plasma concentrations of all analytes following administration of recommended clinical CBD doses. Further, the method enabled their quantification also in another aqueous matrix (Papers II and III).

The *in vitro* metabolic studies in human liver microsomes provided CBD metabolism profiles when investigated alone and co-incubated with various antiseizure medications (ASMs). The CBD depletion rate constant was concentration-dependent, indicating that CBD metabolism reaches saturation, or CBD possibly inhibit its own metabolism. ASMs able to inhibit either CYP3A4 or CYP2C19, such as stiripentol, significantly decreased CBD metabolism. On the other hand, ASMs CYP3A4 substrates marginally affect CBD metabolism, even when combining CBD with up to four ASMs CYP3A4 substrates at the same time. It was clear that ASMs non-CYP450 substrates showed no influence on CBD *in vitro* metabolism, implying these ASMs may not increase CBD *in vivo* exposure when combined together. The study suggested that a combination of CBD and stiripentol could markedly increase CBD exposure *in vivo*. However, stiripentol could at the same time cause a decrease in 7-OH-CBD formation. Unlike the impact on CBD metabolism, ASMs CYP3A4 substrates could markedly decrease 7-OH-CBD depletion. According to these results, co-medication with a CYP3A4 inhibitor could be one effective approach to effectively increase both CBD and 7-OH-CBD exposure. Moderate-activity CYP2C19 genotypes did not cause a marked decrease in CBD metabolism, indicating marginal clinical impact on CBD *in vivo* exposure.

The *in vitro* study in human iPSC-derived 3D neural cultures gave preliminary information on effective CBD antiseizure and neurotoxic concentrations. This information is important and should be considered in clinical practice when

titrating CBD dose in order to reach the effective concentration but not exceed the neurotoxic levels.

The developed PBPK model as a useful predictive tool, together with the obtained *in vitro* outcomes as the input parameters, could potentially forecast CBD concentration-time profiles following CBD administration with or without drug-drug interactions. In addition, the model could be helpful particularly for children. Further the model could be applied for predicting CBD exposure or individualizing CBD dose, such as those who are receiving certain ASMs combinations.

7 FUTURE PERSPECTIVES

At the time working on this thesis began, the pharmacokinetic and drug-drug interactions profiles of CBD and its active metabolite 7-OH-CBD were fairly unknown although CBD has been an approved antiseizure medication (ASM). This thesis therefore investigated the metabolism of these compounds *in vitro* in order to use the gained knowledge for clinical application.

A possible autoinhibition of CBD is still unclear and more investigation is required, since it is a factor that could improve prediction of steady state exposure more precisely.

Further development of the PBPK model may improve its predictive performance. Since the model did not perform well for multiple dosing (underprediction), other factors, such as autoinhibition or substrate inhibition, may be involved. If CBD should be proven to exhibit autoinhibition or time-dependent enzyme inhibition, such parameters should be included in the model and validation repeated.

In this thesis the effect of CBD alone in cultured human iPSC-derived neurons was studied. However, CBD is not approved as monotherapy but must be combined to other ASMs. The combined effects of ASM(s) and CBD is also of interest to further investigate in the same model to obtain more knowledge if combinations have synergistic, additive, or antagonistic effects. One simple approach to investigate the combined effect of CBD and ASMs is to use isobolographic analysis.

The pharmacokinetic/pharmacodynamic models, such as E_{max} model, is also of interest to be further studied to predict CBD efficacy (e.g., seizure reduction) from the concentrations (e.g., steady-state trough plasma concentration). This work requires sufficient clinical data from the literature or to conduct clinical studies.

Clinical pediatric studies designed to better inform on CBD and 7-OH-CBD concentration-effect relationships at steady-state by population PKPD modelling in varying ASM combination regimens would be desirable.

ACKNOWLEDGEMENT

Almost all works presented in this thesis were performed at the Unit for Pharmacokinetics and Drug metabolism, Department of Pharmacology, and at Department of Physiology, Institute of Neuroscience and Physiology, Sahlgrenska Academy, University of Gothenburg, Sweden.

I am deeply grateful to everyone who has involved, assisted and supported me in every way throughout five years of my studies until I achieved my goals. I really would like to express my special gratitude to all of you:

To my supervisor **Professor Dr. Michael Ashton** for accepting me as PhD student immediately after receiving my CV. During my five-year working here, I have learned a great deal of knowledge on pharmacokinetics from you. Your expert advice has greatly improved the quality of my works. You are a great pharmacokinetic source.

To **Dr. Sofia Birgersson**, my co-supervisor, who provided me with kind support in almost everything during my PhD here. You taught me the principles of LC-MS/MS and how to use it. You also introduced me to pharmacokinetic/pharmacodynamic modelling. Thank you for assisting me in improving my writing skill.

To **Dr. Sebastian Illes**, my co-supervisor for introducing me to neurological research using MEA technology. It is a new world to me, both interesting and useful for my future research. I have learned so much from you.

To **Professor Dr. Pär Matsson**, my co-supervisor, who provided great and useful comments on my work.

To **Associate Professor Dr. Henrik Seth**, my co-supervisor, who gave me helpful comments on my PhD project performed in iPSC-derived neurons.

Additionally, I would like to thank all the members in PKDM group with whom I had a wonderful time during my PhD. **Angela Äbelö**, you spent your time giving me the special lectures on pharmacokinetics and pharmacodynamics. I really appreciate it. **Emma Eckernäs**, you taught me to use HPLC-MS which was an important part of my thesis, as well as laboratory equipment. **Emma Inganäs**, you showed me where the cafeteria was located on my first day in the lab, and helped me to install or fix the software. **Mikael**

Boberg, you are very kind to help me build a PKPD model. **Antonio Carlesso**, who has a positive attitude and searched for new restaurants for us. **Jesper Sundell**, for helping me connect the printer on my first day and for teaching me the basic knowledge on pharmacokinetic modelling. **Erik Arthursson**, thank you for spending your valuable time to help me perform the experiments on iPSC-derived neurons and explain the technical terms in electrophysiology to me. **Mylan Eklund**, for your kind helps in searching information about cell culture experiments. **Alexis Rugamba**, my office mate who brought me a piece of bread at lunch time. **Ruwei Yao**, for joining Antonio and me for a fancy lunch almost every time. **Kurt-Jürgen Hoffmann**, for your expertise in chemistry and your guidance in bioanalysis. Thank you, **everyone in the Department of Pharmacology**, it was great for me to spend time with all of you here. **Maria Björkevik**, thank you for your administrative assistance.

I would like to give a special thanks to **Taylor & Francis Group** for granting permission to reproduce my non-open access research article and include it in my printed thesis.

I also would like to thank the **Royal Thai Government** for the scholarship throughout my PhD studies.

Finally, I would like to thank my family for their kind support from Thailand during my studies in Sweden.

REFERENCES

1. Biset G, Abebaw N, Gebeyehu NA, Estifanos N, Birrie E, Tegegne KD. Prevalence, incidence, and trends of epilepsy among children and adolescents in Africa: a systematic review and meta-analysis. BMC Public Health. 2024;24(1):771.
2. Katyayan A, Diaz-Medina G. Epilepsy: Epileptic Syndromes and Treatment. Neurol Clin. 2021;39(3):779-95.
3. Fisher RS. The New Classification of Seizures by the International League Against Epilepsy 2017. Curr Neurol Neurosci Rep. 2017;17(6):48.
4. Costagliola G, Depietri G, Michev A, Riva A, Foiadelli T, Savasta S, et al. Targeting Inflammatory Mediators in Epilepsy: A Systematic Review of Its Molecular Basis and Clinical Applications. Front Neurol. 2022;13:741244.
5. Scheffer IE, Berkovic S, Capovilla G, Connolly MB, French J, Guilhoto L, et al. ILAE classification of the epilepsies: Position paper of the ILAE Commission for Classification and Terminology. Epilepsia. 2017;58(4):512-21.
6. Fisher RS, Cross JH, French JA, Higurashi N, Hirsch E, Jansen FE, et al. Operational classification of seizure types by the International League Against Epilepsy: Position Paper of the ILAE Commission for Classification and Terminology. Epilepsia. 2017;58(4):522-30.
7. Anwar H, Khan QU, Nadeem N, Pervaiz I, Ali M, Cheema FF. Epileptic seizures. Discoveries (Craiova). 2020;8(2):e110.
8. He Z, Li Y, Zhao X, Li B. Dravet syndrome: Advances in etiology, clinical presentation, and treatment. Epilepsy Res. 2022;188:107041.
9. Anwar A, Saleem S, Patel UK, Arumaithurai K, Malik P. Dravet Syndrome: An Overview. Cureus. 2019;11(6):e5006.
10. Favero M, Sotuyo NP, Lopez E, Kearney JA, Goldberg EM. A Transient Developmental Window of Fast-Spiking Interneuron Dysfunction in a Mouse Model of Dravet Syndrome. J Neurosci. 2018;38(36):7912-27.
11. Capitano F, Kuchenbuch M, Lavigne J, Chaptoukaev H, Zuluaga MA, Lorenzi M, et al. Preictal dysfunctions of inhibitory interneurons paradoxically lead to their rebound hyperactivity and to low-voltage-fast onset seizures in Dravet syndrome. Proc Natl Acad Sci U S A. 2024;121(23):e2316364121.
12. Bureau M, Dalla Bernardina B. Electroencephalographic characteristics of Dravet syndrome. Epilepsia. 2011;52 Suppl 2:13-23.
13. Minato E, Myers KA. Age-related evolution of EEG in Dravet syndrome: Meta-analysis of 155 patients. Seizure. 2021;91:108-11.

14. Strzelczyk A, Schubert-Bast S. A Practical Guide to the Treatment of Dravet Syndrome with Anti-Seizure Medication. CNS Drugs. 2022;36(3):217-37.
15. Gao C, Pielas M, Jiao F, Mei D, Wang X, Kotulska K, et al. Epilepsy in Dravet Syndrome-Current and Future Therapeutic Opportunities. J Clin Med. 2023;12(7):2532.
16. Wirrell EC, Nabbout R. Recent Advances in the Drug Treatment of Dravet Syndrome. CNS Drugs. 2019;33(9):867-81.
17. Verrotti A, Striano P, Iapadre G, Zagaroli L, Bonanni P, Coppola G, et al. The pharmacological management of Lennox-Gastaut syndrome and critical literature review. Seizure. 2018;63:17-25.
18. Asadi-Pooya AA. Lennox-Gastaut syndrome: a comprehensive review. Neurol Sci. 2018;39(3):403-14.
19. Strzelczyk A, Schubert-Bast S. Expanding the Treatment Landscape for Lennox-Gastaut Syndrome: Current and Future Strategies. CNS Drugs. 2021;35(1):61-83.
20. Arzimanoglou A, French J, Blume WT, Cross JH, Ernst JP, Feucht M, et al. Lennox-Gastaut syndrome: a consensus approach on diagnosis, assessment, management, and trial methodology. Lancet Neurol. 2009;8(1):82-93.
21. Jahngir MU, Ahmad MQ, Jahangir M. Lennox-Gastaut Syndrome: In a Nutshell. Cureus. 2018;10(8):e3134.
22. Cross JH, Auvin S, Falip M, Striano P, Arzimanoglou A. Expert Opinion on the Management of Lennox-Gastaut Syndrome: Treatment Algorithms and Practical Considerations. Front Neurol. 2017;8:505.
23. Zhang L, Wang J, Wang C. Efficacy and safety of antiseizure medication for Lennox-Gastaut syndrome: a systematic review and network meta-analysis. Dev Med Child Neurol. 2022;64(3):305-13.
24. Montouris G, Aboumatar S, Burdette D, Kothare S, Kuzniecky R, Rosenfeld W, et al. Expert opinion: Proposed diagnostic and treatment algorithms for Lennox-Gastaut syndrome in adult patients. Epilepsy Behav. 2020;110:107146.
25. Feucht M, Brantner-Inthaler S. Gamma-vinyl-GABA (vigabatrin) in the therapy of Lennox-Gastaut syndrome: an open study. Epilepsia. 1994;35(5):993-8.
26. von Wrede R, Helmstaedter C, Surges R. Cannabidiol in the Treatment of Epilepsy. Clin Drug Investig. 2021;41(3):211-20.
27. Dabora SL, Jozwiak S, Franz DN, Roberts PS, Nieto A, Chung J, et al. Mutational analysis in a cohort of 224 tuberous sclerosis patients indicates increased severity of TSC2, compared with TSC1, disease in multiple organs. Am J Hum Genet. 2001;68(1):64-80.
28. Crocq MA. History of cannabis and the endocannabinoid system. Dialogues Clin Neurosci. 2020;22(3):223-8.

29. Nelson KM, Bisson J, Singh G, Graham JG, Chen SN, Friesen JB, et al. The Essential Medicinal Chemistry of Cannabidiol (CBD). J Med Chem. 2020;63(21):12137-55.
30. Stella B, Baratta F, Della Pepa C, Arpicco S, Gastaldi D, Dosio F. Cannabinoid Formulations and Delivery Systems: Current and Future Options to Treat Pain. Drugs. 2021;81(13):1513-57.
31. Tabboon P, Pongjanyakul T, Limpongsa E, Jaipakdee N. Mucosal Delivery of Cannabidiol: Influence of Vehicles and Enhancers. Pharmaceutics. 2022;14(8):1687.
32. Koch N, Jennotte O, Gasparrini Y, Vandenbroucke F, Lechanteur A, Evrard B. Cannabidiol aqueous solubility enhancement: Comparison of three amorphous formulations strategies using different type of polymers. Int J Pharm. 2020;589:119812.
33. Grifoni L, Vanti G, Donato R, Sacco C, Bilia AR. Promising Nanocarriers to Enhance Solubility and Bioavailability of Cannabidiol for a Plethora of Therapeutic Opportunities. Molecules. 2022;27(18).
34. Peres FF, Lima AC, Hallak JEC, Crippa JA, Silva RH, Abílio VC. Cannabidiol as a Promising Strategy to Treat and Prevent Movement Disorders? Front Pharmacol. 2018;9:482.
35. Atalay S, Jarocka-Karpowicz I, Skrzydlewska E. Antioxidative and Anti-Inflammatory Properties of Cannabidiol. Antioxidants (Basel). 2019;9(1):21.
36. Yamaori S, Ebisawa J, Okushima Y, Yamamoto I, Watanabe K. Potent inhibition of human cytochrome P450 3A isoforms by cannabidiol: role of phenolic hydroxyl groups in the resorcinol moiety. Life Sci. 2011;88(15-16):730-6.
37. Kicman A, Toczek M. The Effects of Cannabidiol, a Non-Intoxicating Compound of Cannabis, on the Cardiovascular System in Health and Disease. Int J Mol Sci. 2020;21(18):6740.
38. Galaj E, Xi Z-X. Possible Receptor Mechanisms Underlying Cannabidiol Effects on Addictive-like Behaviors in Experimental Animals. Int J Mol Sci. 2021;22(1):134.
39. Nicoara C, Fezza F, Maccarrone M. FAAH Modulators from Natural Sources: A Collection of New Potential Drugs. Cells. 2025; 14(7):551.
40. Maa E, Figi P. The case for medical marijuana in epilepsy. Epilepsia. 2014;55(6):783-6.
41. Nabbout R, Thiele EA. The role of cannabinoids in epilepsy treatment: a critical review of efficacy results from clinical trials. Epileptic Disord. 2020;22(S1):23-8.
42. Chico SFV, Diaz DAM, Contreras-Puentes N. Use of cannabidiol in the treatment of drug-refractory epilepsy in children and young adults: A systematic review. J Neurosci Rural Pract. 2024;15(2):203-10.

43. Devinsky O, Marsh E, Friedman D, Thiele E, Laux L, Sullivan J, et al. Cannabidiol in patients with treatment-resistant epilepsy: an open-label interventional trial. Lancet Neurol. 2016;15(3):270-8.
44. Arnold JC, McCartney D, Suraev A, McGregor IS. The safety and efficacy of low oral doses of cannabidiol: An evaluation of the evidence. Clin Transl Sci. 2023;16(1):10-30.
45. Park YD, Linder DF, Pope J, Flamini JR, Moretz K, Diamond MP, et al. Long-term efficacy and safety of cannabidiol (CBD) in children with treatment-resistant epilepsy: Results from a state-based expanded access program. Epilepsy Behav. 2020;112:107474.
46. Cross JH, Cock H. A perspective on cannabinoids for treating epilepsy: Do they really change the landscape? Neuropharmacology. 2020;170:107861.
47. Gray RA, Whalley BJ. The proposed mechanisms of action of CBD in epilepsy. Epileptic Disord. 2020;22(S1):10-5.
48. Meza RC, Ancatén-González C, Chiu CQ, Chávez AE. Transient Receptor Potential Vanilloid 1 Function at Central Synapses in Health and Disease. Front Cell Neurosci. 2022;16:864828.
49. Mirlohi S, Bladen C, Santiago MJ, Arnold JC, McGregor I, Connor M. Inhibition of human recombinant T-type calcium channels by phytocannabinoids in vitro. Br J Pharmacol. 2022;179(15):4031-43.
50. Ghovanloo MR, Shuart NG, Mezeyova J, Dean RA, Ruben PC, Goodchild SJ. Inhibitory effects of cannabidiol on voltage-dependent sodium currents. J Biol Chem. 2018;293(43):16546-58.
51. Yu Y, Yang Z, Jin B, Qin X, Zhu X, Sun J, et al. Cannabidiol inhibits febrile seizure by modulating AMPA receptor kinetics through its interaction with the N-terminal domain of GluA1/GluA2. Pharmacol Res. 2020;161:105128.
52. Ujvary I, Lopata A. Phenytoin-like antiepileptic effect of cannabidiol and related phytocannabinoid metabolites: Structural insights from molecular modeling. J Biomed Res Rev. 2020;3:32-40.
53. Ujváry I, Hanuš L. Human Metabolites of Cannabidiol: A Review on Their Formation, Biological Activity, and Relevance in Therapy. Cannabis Cannabinoid Res. 2016;1(1):90-101.
54. Jones NA, Hill AJ, Smith I, Bevan SA, Williams CM, Whalley BJ, et al. Cannabidiol displays antiepileptiform and antiseizure properties in vitro and in vivo. J Pharmacol Exp Ther. 2010;332(2):569-77.
55. Ghovanloo MR, Shuart NG, Mezeyova J, Dean RA, Ruben PC, Goodchild SJ. Inhibitory Effects of Cannabidiol on Voltage-Dependent Sodium Currents. J Biol Chem. 2018;293:16546.
56. Ross HR, Napier I, Connor M. Inhibition of recombinant human T-type calcium channels by Delta9-tetrahydrocannabinol and cannabidiol. J Biol Chem. 2008;283(23):16124-34.

57. dos Santos RG, Hallak JE, Leite JP, Zuardi AW, Crippa JA. Phytocannabinoids and epilepsy. J Clin Pharm Ther. 2015;40(2):135-43.
58. Consroe P, Wolkin A. Cannabidiol--antiepileptic drug comparisons and interactions in experimentally induced seizures in rats. J Pharmacol Exp Ther. 1977;201(1):26-32.
59. Golub V, Ramakrishnan S, Reddy DS. Isobolographic analysis of adjunct antiseizure activity of the FDA-approved cannabidiol with neurosteroids and benzodiazepines in adult refractory focal onset epilepsy. Exp Neurol. 2023;360:114294.
60. Rana RR, Rajasekaran K, Knappertz V, Gray RA. Pharmacodynamic synergism contributes to the antiseizure action of cannabidiol and clobazam. Exp Neurol. 2023;360:114286.
61. Bansal S, Maharao N, Paine MF, Unadkat JD. Predicting the Potential for Cannabinoids to Precipitate Pharmacokinetic Drug Interactions via Reversible Inhibition or Inactivation of Major Cytochromes P450. Drug Metab Dispos. 2020;48(10):1008-17.
62. Taylor L, Gidal B, Blakey G, Tayo B, Morrison G. A Phase I, Randomized, Double-Blind, Placebo-Controlled, Single Ascending Dose, Multiple Dose, and Food Effect Trial of the Safety, Tolerability and Pharmacokinetics of Highly Purified Cannabidiol in Healthy Subjects. CNS Drugs. 2018;32(11):1053-67.
63. Millar SA, Maguire RF, Yates AS, O'Sullivan SE. Towards Better Delivery of Cannabidiol (CBD). Pharmaceuticals (Basel). 2020;13(9).
64. Helen Chan O, Stewart BH. Physicochemical and drug-delivery considerations for oral drug bioavailability. Drug Discov Today. 1996;1(11):461-73.
65. CBD-OS FOR THE TREATMENT OF LENNOX-GASTAUT SYNDROME AND DRAVET SYNDROME FDA ADVISORY COMMITTEE MEETING BRIEFING DOCUMENT PERIPHERAL AND CENTRAL NERVOUS SYSTEM DRUG ADVISORY COMMITTEE 2018 [cited 2026 Jan 5]. Available from: https://www.fda.gov/files/advisory%20committees/published/GW-Briefing-Information-for-the-April-19-2018-Meeting-of-the-Peripheral-and-Central-Nervous-System-Drugs-Advisory-Committee.pdf.
66. Williams NNB, Ewell TR, Abbotts KSS, Harms KJ, Woelfel KA, Dooley GP, et al. Comparison of Five Oral Cannabidiol Preparations in Adult Humans: Pharmacokinetics, Body Composition, and Heart Rate Variability. Pharmaceuticals (Basel). 2021;14(1):35.
67. Kolli AR, Hoeng J. Cannabidiol Bioavailability Is Nonmonotonic with a Long Terminal Elimination Half-Life: A Pharmacokinetic Modeling-Based Analysis. Cannabis Cannabinoid Res. 2025;10(1):81-91.

68. Sitovs A, Logviss K, Petersone L, Mohylyuk V. Oral delivery of cannabidiol: Revealing the formulation and absorption challenges. Journal of Drug Delivery Science and Technology. 2023;92:105316.
69. Lim SY, Sharan S, Woo S. Model-Based Analysis of Cannabidiol Dose-Exposure Relationship and Bioavailability. Pharmacotherapy. 2020;40(4):291-300.
70. Silva GD, Del Guerra FB, de Oliveira Lelis M, Pinto LF. Cannabidiol in the Treatment of Epilepsy: A Focused Review of Evidence and Gaps. Front Neurol. 2020;11:531939.
71. O'Sullivan SE, Jensen SS, Kolli AR, Nikolajsen GN, Bruun HZ, Hoeng J. Strategies to Improve Cannabidiol Bioavailability and Drug Delivery. Pharmaceuticals (Basel). 2024;17(2):244.
72. Lucas CJ, Galettis P, Schneider J. The pharmacokinetics and the pharmacodynamics of cannabinoids. Br J Clin Pharmacol. 2018;84(11):2477-82.
73. Ohlsson A, Lindgren JE, Andersson S, Agurell S, Gillespie H, Hollister LE. Single-dose kinetics of deuterium-labelled cannabidiol in man after smoking and intravenous administration. Biomed Environ Mass Spectrom. 1986;13(2):77-83.
74. Gronewold A, Skopp G. A preliminary investigation on the distribution of cannabinoids in man. Forensic Sci Int. 2011;210(1-3):e7-e11.
75. Tayo B, Taylor L, Sahebkar F, Morrison G. A Phase I, Open-Label, Parallel-Group, Single-Dose Trial of the Pharmacokinetics, Safety, and Tolerability of Cannabidiol in Subjects with Mild to Severe Renal Impairment. Clin Pharmacokinet. 2020;59(6):747-55.
76. Taylor L, Crockett J, Tayo B, Morrison G. A Phase 1, Open-Label, Parallel-Group, Single-Dose Trial of the Pharmacokinetics and Safety of Cannabidiol (CBD) in Subjects With Mild to Severe Hepatic Impairment. J Clin Pharmacol. 2019;59(8):1110-9.
77. Schwope DM, Karschner EL, Gorelick DA, Huestis MA. Identification of recent cannabis use: whole-blood and plasma free and glucuronidated cannabinoid pharmacokinetics following controlled smoked cannabis administration. Clin Chem. 2011;57(10):1406-14.
78. Schwilke EW, Karschner EL, Lowe RH, Gordon AM, Cadet JL, Herning RI, et al. Intra- and intersubject whole blood/plasma cannabinoid ratios determined by 2-dimensional, electron impact GC-MS with cryofocusing. Clin Chem. 2009;55(6):1188-95.
79. Calapai F, Cardia L, Sorbara EE, Navarra M, Gangemi S, Calapai G, et al. Cannabinoids, Blood–Brain Barrier, and Brain Disposition. Pharmaceutics. 2020;12(3):265.
80. Beers JL, Fu D, Jackson KD. Cytochrome P450-Catalyzed Metabolism of Cannabidiol to the Active Metabolite 7-Hydroxy-Cannabidiol. Drug Metab Dispos. 2021;49(10):882-91.

81. Landmark CJ, Brandl U. Pharmacology and drug interactions of cannabinoids. Epileptic Disord. 2020;22(S1):16-22.
82. Ochi M, Kohnosuke K, Jun-ichi Y, and Endo H. Bottom-up physiologically based pharmacokinetic modelling for predicting the human pharmacokinetic profiles of the ester prodrug MGS0274 and its active metabolite MGS0008, a metabotropic glutamate 2/3 receptor agonist. Xenobiotica. 2022;52(2):119-28.
83. Zhuang X, Lu C. PBPK modeling and simulation in drug research and development. Acta Pharm Sin B. 2016;6(5):430-40.
84. Jones H, Rowland-Yeo K. Basic concepts in physiologically based pharmacokinetic modeling in drug discovery and development. CPT Pharmacometrics Syst Pharmacol. 2013;2(8):e63.
85. Tsamandouras N, Rostami-Hodjegan A, Aarons L. Combining the 'bottom up' and 'top down' approaches in pharmacokinetic modelling: fitting PBPK models to observed clinical data. Br J Clin Pharmacol. 2015;79(1):48-55.
86. Hartmanshenn C, Scherholz M, Androulakis IP. Physiologically-based pharmacokinetic models: approaches for enabling personalized medicine. J Pharmacokinet Pharmacodyn. 2016;43(5):481-504.
87. Tylutki Z, Polak S, Wiśniowska B. Top-down, Bottom-up and Middle-out Strategies for Drug Cardiac Safety Assessment via Modeling and Simulations. Current Pharmacology Reports. 2016;2(4):171-7.
88. Morris G, Avoli M, Bernard C, Connor K, de Curtis M, Dulla CG, et al. Can in vitro studies aid in the development and use of antiseizure therapies? A report of the ILAE/AES Joint Translational Task Force. Epilepsia. 2023;64(10):2571-85.
89. Zhao C, Rollo B, Shahid Javaid M, Huang Z, He W, Xu H, et al. An integrated in vitro human iPSCs-derived neuron and in vivo animal approach for preclinical screening of anti-seizure compounds. J Adv Res. 2024;64:249-62.
90. Oblasov I, Idzhilova O, Balaban P, Nikitin E. Cell culture models for epilepsy research and treatment. Explor Med. 2024;5(1):65-75.
91. Dulla CG, Janigro D, Jiruska P, Raimondo JV, Ikeda A, Lin CK, et al. How do we use in vitro models to understand epileptiform and ictal activity? A report of the TASK1-WG4 group of the ILAE/AES Joint Translational Task Force. Epilepsia Open. 2018;3(4):460-73.
92. Lévesque M, Avoli M. The kainic acid model of temporal lobe epilepsy. Neurosci Biobehav Rev. 2013;37(10 Pt 2):2887-99.
93. de Curtis M, Uva L, Gnatkovsky V, Librizzi L. Potassium dynamics and seizures: Why is potassium ictogenic? Epilepsy Res. 2018;143:50-9.
94. Köhling R, Wolfart J. Potassium Channels in Epilepsy. Cold Spring Harb Perspect Med. 2016;6(5):a022871.

95. Cho Y-J, Kim H, Kim W-J, Chung S, Kim Y-H, Cho I, et al. Trafficking patterns of NMDA and GABAA receptors in a Mg2+-free cultured hippocampal neuron model of status epilepticus. Epilepsy Res. 2017;136:143-8.
96. Isaev D, Ivanchick G, Khmyz V, Isaeva E, Savrasova A, Krishtal O, et al. Surface charge impact in low-magnesium model of seizure in rat hippocampus. J Neurophysiol. 2012;107(1):417-23.
97. Myers TL, Gonzalez OC, Stein JB, Bazhenov M. Characterizing Concentration-Dependent Neural Dynamics of 4-Aminopyridine-Induced Epileptiform Activity. Epilepsy J. 2018;4(2):128.
98. Reddy DS, Kuruba R. Experimental models of status epilepticus and neuronal injury for evaluation of therapeutic interventions. Int J Mol Sci. 2013;14(9):18284-318.
99. Heuzeroth H, Wawra M, Fidzinski P, Dag R, Holtkamp M. The 4-Aminopyridine Model of Acute Seizures in vitro Elucidates Efficacy of New Antiepileptic Drugs. Front Neurosci. 2019;13:677.
100. Siniscalchi A, Calabresi P, Mercuri NB, Bernardi G. Epileptiform discharge induced by 4-aminopyridine in magnesium-free medium in neocortical neurons: physiological and pharmacological characterization. Neuroscience. 1997;81(1):189-97.
101. Gonzalez-Sulser A, Wang J, Queenan BN, Avoli M, Vicini S, Dzakpasu R. Hippocampal neuron firing and local field potentials in the in vitro 4-aminopyridine epilepsy model. J Neurophysiol. 2012;108(9):2568-80.
102. Gonzalez-Sulser A, Wang J, Motamedi GK, Avoli M, Vicini S, Dzakpasu R. The 4-aminopyridine in vitro epilepsy model analyzed with a perforated multi-electrode array. Neuropharmacology. 2011;60(7):1142-53.
103. Nascimento FA, Andrade DM. Myoclonus epilepsy and ataxia due to potassium channel mutation (MEAK) is caused by heterozygous KCNC1 mutations. Epileptic Disord. 2016;18(S2):135-8.
104. Gunning B, Mazurkiewicz-Bełdzińska M, Chin RFM, Bhathal H, Nortvedt C, Dunayevich E, et al. Cannabidiol in conjunction with clobazam: analysis of four randomized controlled trials. Acta Neurol Scand. 2021;143(2):154-63.
105. Bioanalytical Method Validation Guidance for Industry [Internet]. 2018 [cited July 20, 2021]. Available from: https://www.fda.gov/files/drugs/published/Bioanalytical-Method-Validation-Guidance-for-Industry.pdf.
106. Beers JL, Fu D, Jackson KD. Cytochrome P450-Catalyzed Metabolism of Cannabidiol to the Active Metabolite 7-Hydroxy-Cannabidiol. Drug Metab Dispos. 2021;49(10):882-91.
107. Bansal S, Paine MF, Unadkat JD. Comprehensive Predictions of Cytochrome P450 (P450)-Mediated In Vivo Cannabinoid-Drug Interactions Based on Reversible and Time-Dependent P450 Inhibition in Human Liver Microsomes. Drug Metab Dispos. 2022;50(4):351-60.

108. Back HM, Yun HY, Kim SK, Kim JK. Beyond the Michaelis-Menten: Accurate Prediction of In Vivo Hepatic Clearance for Drugs With Low K(M). Clin Transl Sci. 2020;13(6):1199-207.
109. Izsak J, Seth H, Andersson M, Vizlin-Hodzic D, Theiss S, Hanse E, et al. Robust Generation of Person-Specific, Synchronously Active Neuronal Networks Using Purely Isogenic Human iPSC-3D Neural Aggregate Cultures. Front Neurosci. 2019;13:351.
110. Izsak J, Seth H, Iljin M, Theiss S, Ågren H, Funa K, et al. Differential acute impact of therapeutically effective and overdose concentrations of lithium on human neuronal single cell and network function. Transl Psychiatry. 2021;11(1):281.
111. Verscheijden LFM, Koenderink JB, de Wildt SN, Russel FGM. Development of a physiologically-based pharmacokinetic pediatric brain model for prediction of cerebrospinal fluid drug concentrations and the influence of meningitis. PLoS Comput Biol. 2019;15(6):e1007117.
112. Kasteel EEJ, Lautz LS, Culot M, Kramer NI, Zwartsen A. Application of in vitro data in physiologically-based kinetic models for quantitative in vitro-in vivo extrapolation: A case-study for baclofen. Toxicol In Vitro. 2021;76:105223.
113. Chang HP, Kim SJ, Wu D, Shah K, Shah DK. Age-Related Changes in Pediatric Physiology: Quantitative Analysis of Organ Weights and Blood Flows. AAPS J. 2021;23(3):50.
114. Barter ZE, Chowdry JE, Harlow JR, Snawder JE, Lipscomb JC, Rostami-Hodjegan A. Covariation of human microsomal protein per gram of liver with age: absence of influence of operator and sample storage may justify interlaboratory data pooling. Drug Metab Dispos. 2008;36(12):2405-9.
115. Berton M, Bettonte S, Stader F, Battegay M, Marzolini C. Repository Describing the Anatomical, Physiological, and Biological Changes in an Obese Population to Inform Physiologically Based Pharmacokinetic Models. Clin Pharmacokinet. 2022;61(9):1251-70.
116. Barras M, Legg A. Drug dosing in obese adults. Aust Prescr. 2017;40(5):189-93.
117. Haddad S, Restieri C, Krishnan K. Characterization of age-related changes in body weight and organ weights from birth to adolescence in humans. J Toxicol Environ Health A. 2001;64(6):453-64.
118. Poulin P, Theil FP. Prediction of pharmacokinetics prior to in vivo studies. 1. Mechanism-based prediction of volume of distribution. J Pharm Sci. 2002;91(1):129-56.
119. Holt K, Ye M, Nagar S, Korzekwa K. Prediction of Tissue-Plasma Partition Coefficients Using Microsomal Partitioning: Incorporation into Physiologically based Pharmacokinetic Models and Steady-State Volume of Distribution Predictions. Drug Metab Dispos. 2019;47(10):1050-60.

120. Yim DS, Choi S. Predicting human pharmacokinetics from preclinical data: volume of distribution. Transl Clin Pharmacol. 2020;28(4):169-74.
121. Brussee JM, Yu H, Krekels EHJ, Palić S, Brill MJE, Barrett JS, et al. Characterization of Intestinal and Hepatic CYP3A-Mediated Metabolism of Midazolam in Children Using a Physiological Population Pharmacokinetic Modelling Approach. Pharm Res. 2018;35(9):182.
122. Schoedel KA, Szeto I, Setnik B, Sellers EM, Levy-Cooperman N, Mills C, et al. Abuse potential assessment of cannabidiol (CBD) in recreational polydrug users: A randomized, double-blind, controlled trial. Epilepsy Behav. 2018;88:162-71.
123. Morrison G, Crockett J, Blakey G, Sommerville K. A Phase 1, Open-Label, Pharmacokinetic Trial to Investigate Possible Drug-Drug Interactions Between Clobazam, Stiripentol, or Valproate and Cannabidiol in Healthy Subjects. Clin Pharmacol Drug Dev. 2019;8(8):1009-31.
124. Zhang Q, Melchert PW, Markowitz JS. Pharmacokinetic Variability of Oral Cannabidiol and Its Major Metabolites after Short-Term High-Dose Exposure in Healthy Subjects. Med Cannabis Cannabinoids. 2024;7(1):1-9.
125. Devinsky O, Patel AD, Thiele EA, Wong MH, Appleton R, Harden CL, et al. Randomized, dose-ranging safety trial of cannabidiol in Dravet syndrome. Neurology. 2018;90(14):e1204.
126. Wheless JW, Dlugos D, Miller I, Oh DA, Parikh N, Phillips S, et al. Pharmacokinetics and Tolerability of Multiple Doses of Pharmaceutical-Grade Synthetic Cannabidiol in Pediatric Patients with Treatment-Resistant Epilepsy. CNS Drugs. 2019;33(6):593-604.
127. Ye M, Nagar S, Korzekwa K. A physiologically based pharmacokinetic model to predict the pharmacokinetics of highly protein-bound drugs and the impact of errors in plasma protein binding. Biopharm Drug Dispos. 2016;37(3):123-41.
128. Contin M, Mohamed S, Santucci M, Lodi MAM, Russo E, Mecarelli O, et al. Cannabidiol in Pharmacoresistant Epilepsy: Clinical Pharmacokinetic Data From an Expanded Access Program. Front Pharmacol. 2021;12:637801.
129. Bansal S, Ladumor MK, Paine MF, Unadkat JD. A Physiologically-Based Pharmacokinetic Model for Cannabidiol in Healthy Adults, Hepatically-Impaired Adults, and Children. Drug Metab Dispos. 2023;51(6):743-52.
130. Schultz HB, Hosseini A, McLachlan AJ, Reuter SE. Population Pharmacokinetics of Oral-Based Administration of Cannabidiol in Healthy Adults: Implications for Drug Development. Cannabis Cannabinoid Res. 2023;8(5):877-86.
131. Sitovs A, Logviss K, Lauberte L, Mohylyuk V. Oral delivery of cannabidiol: Revealing the formulation and absorption challenges. J Drug Deliv Sci Technol. 2024;92:105316.